UNIVERSITY OF CALIFORNIA

Santa Barbara

Photoactivated and Hydrogen Peroxide-Mediated Carbon Monoxide-Releasing Molecules (CORMs)

A Thesis submitted in partial satisfaction of the

requirements for the degree Master of Science

in Chemistry

by

Sheila S. Kulkarni

Committee in charge:

Professor Peter Ford, Chair

Professor Mahdi Abu-Omar

Professor Alison Butler

June 2023

The thesis of Sheila S. Kulkarni is approved.

_____

Alison Butler

_____

Mahdi Abu-Omar

_____

Peter Ford, Committee Chair

June 2023

Photoactivated and Hydrogen Peroxide-Mediated Carbon Monoxide-Releasing Molecules (CORMs)

by

Sheila S. Kulkarni

ACKNOWLEDGEMENTS

I wish to acknowledge my advisor, Dr. Peter C. Ford, for his incredible mentorship, support, and kindness for me over the past few years. I also appreciate my committee, Professors Butler and Abu-Omar, very much for their guidance. I thank my partners for their tireless support, advice, and care for me, and the comrades and friends I have made in Santa Barbara. La lucha sigue!

ABSTRACT

Photoactivated and Hydrogen Peroxide-Mediated Carbon Monoxide-Releasing Molecules (CORMs)

by

Sheila S. Kulkarni

Carbon monoxide (CO), as a small, signaling molecule in mammals, has shown healing effects when applied externally. Targeted internal delivery of CO through a variety of methods is of interest; in this work, we seek to develop many strategies for internal CO release from inorganic platforms. We touch on a family of heterobimetallic group 7 complexes for potential long-wavelength photorelease of CO. We also report synthesis and characterization of a manganese complex whose reaction with H_2O_2 would further previous mechanistic studies of CO release in disease states that express reactive oxygen species (ROS). Future work will focus on kinetics studies to refine the mechanism of H_2O_2 triggered CO release from the CORM $Mn(CO)_3$(4,4'-$(COOH)_2$-bpy)Br. By focusing on diverse methods of delivering CO internally, we expand on burgeoning research to use small molecule bioregulators (SMBs) as specialized medicinal agents.

TABLE OF CONTENTS

I. Introduction

Carbon monoxide (CO) is widely understood to be a toxin to human health upon inhalation due to its high affinity for hemoglobin. Preferential binding of hemoglobin to CO depresses its oxygen-carrying capacity, leading to potentially fatal health effects.[1] However, small amounts of CO are produced endogenously for various purposes, namely in the activity of heme oxygenases (HOs).[2] HOs are a class of enzymes which catalyze the breakdown of heme, releasing CO in the process (Figure 1). As such, the therapeutic effects of CO itself are worthy of study.

CO is considered a small molecule bioregulator (SMB), a category which encompasses other small molecules such as NO, O_2, H_2S, and even CS_2.[3,4,5] SMBs are small molecules that play a signaling role in mammalian physiology, and with the exception of O_2, are all produced endogenously.[6] In particular, CO is an SMB of interest because of its unique, yet relatively inert reactivity compared to other gasotransmitters like NO and H_2S. The π-antibonding orbitals that characterize CO's bonding give an affinity towards binding to low-valent transition metals due to the backbonding interaction, a phenomenon in which filled metal-centered orbitals overlap with the empty π* orbitals of CO.[7] This strong association with low-valent transition metals, such as the Fe(II) center in heme, is responsible for CO's reputation as a "silent killer" as well as its unique physiological chemistry.

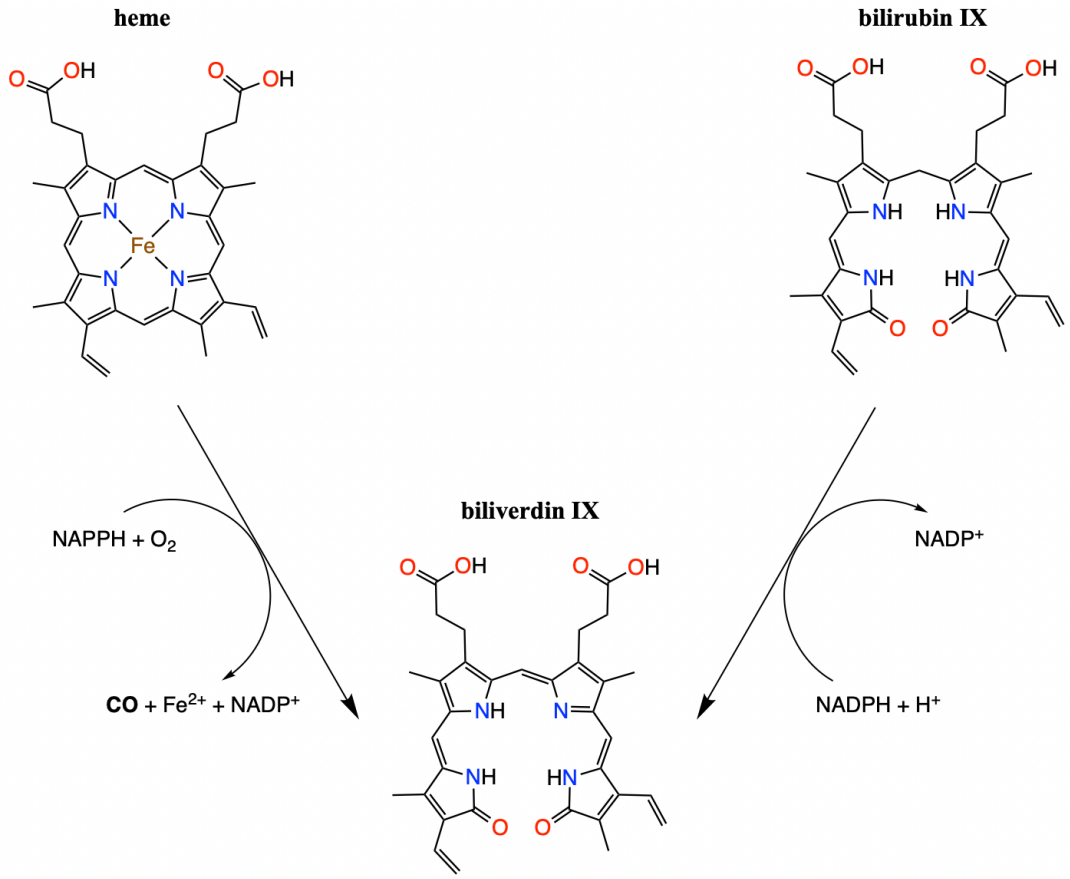

Figure 1. Breakdown of heme catalyzed by heme oxygenases. An equivalent of CO is released upon the oxidation of heme to form biliverdin IX.[2]

SMBs, along with their particular roles and therapeutic potential, have been studied extensively in the past four decades since NO was discovered to play a major role in cardiovascular control and act as a neurotransmitter.[8] The reactions of NO with metal centers in biological systems such as copper and both heme and non-heme iron, present a model for studying CO's physiological impacts in kind. While CO has shown cytoprotective, anti-hypertensive, anti-inflammatory, and vasodilatory effects as illustrated in Figure 2, exogenous application is limited by issues with storage, transport, and CO's aforementioned reactivity with hemoglobin.[9,10] Indeed, CO has shown to exhibit anti-proliferative effects when

applied *in vivo* to various cancer cell lines.[11,12] As such, strategies for targeted internal CO release are needed to explore this SMB's potential for therapy.

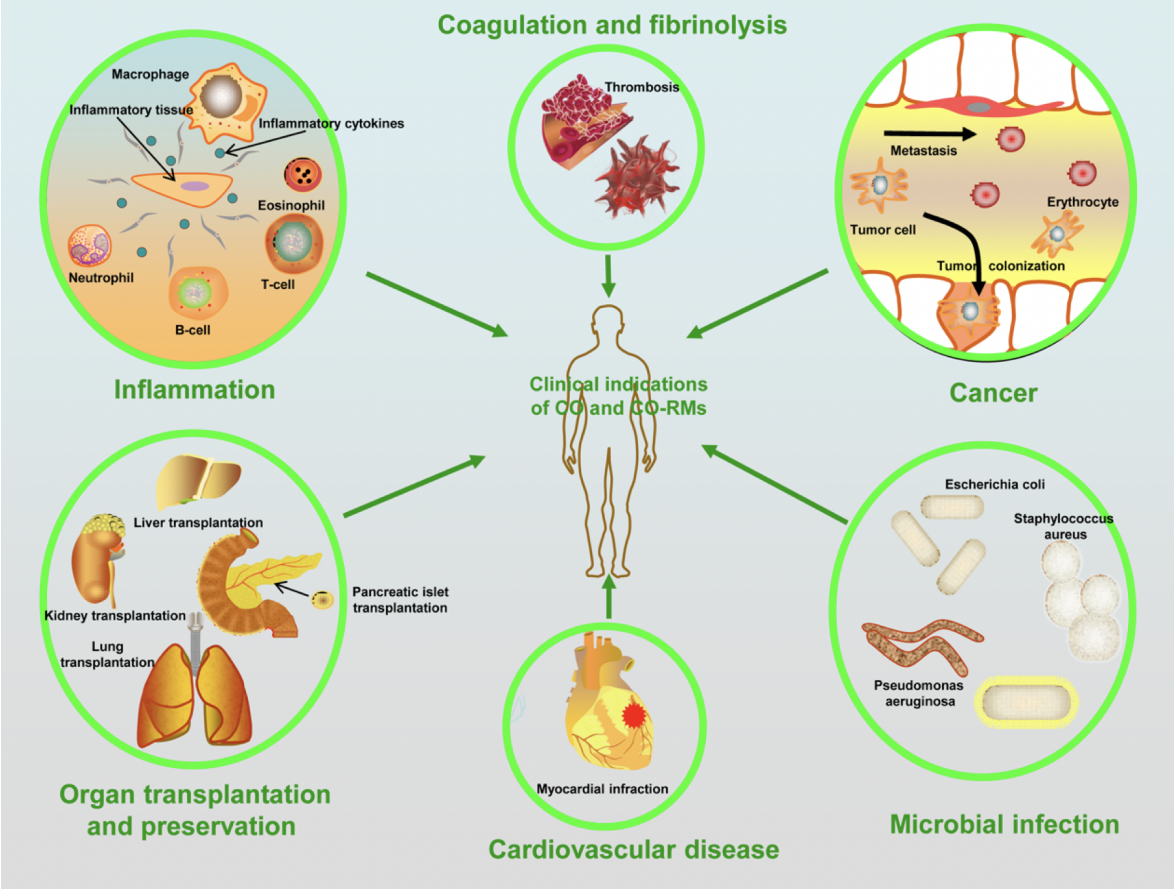

Figure 2. Therapeutic activity of CO-releasing molecules, illustrating the wide-ranging healing potential of CO. Reprinted with permission from Ling, K.; Men, F.; Wang, W-C.; Zhou, Y-Q.; Zhang, H-W.; Ye, D-W. Carbon Monoxide and Its Controlled Release: Therapeutic Application, Detection, and Development of Carbon Monoxide Releasing Molecules (CORMs). *J. Med. Chem.* **2018**, *61*, 2611-2635. DOI: http://doi.org/10.1021/acs.jmedchem.6b01153. Copyright © 2018, American Chemical Society.

Internal release of CO can be carried out using a class of molecules called CORMs, or CO-releasing molecules. In refining these CO delivery strategies, current areas of development are ensuring that these CO-releasing prodrugs are efficient, biologically compatible, minimally toxic, and stable until responding to a particular trigger.[13,14]

One such trigger to release CO from a metal carbonyl is light, a traceless reagent. Photoactivation leads to high spatial and temporal control over CO release, and the ability to measure the quantum yields of CO release from inorganic photoCORMs allows for precise dosage.[15] Metal carbonyls for use as photoCORMs tend to be d^6 metal centers coordinated to polypyridine ligand(s) which impart low-lying π* orbitals. These give rise to metal to ligand charge transfer (MLCT) optical transitions in the visible region, leading to these complexes' vibrant colors.

Another strategy for uncaging CO from inorganic CORMs is activation of the CORM with a reagent present in mammalian systems, such as reactive oxygen species or other small molecules which accumulate in hypoxic tumor sites.[16] Selective binding of CORMs to those particular targets would lead to accumulation of the CORM in those diseased sites, a method to spatially target CO release.

This work will focus on strategies for internal release of CO from group 7 carbonyl complexes featuring chromophore ligands such as bipyridine and derivatives; namely, photoactivity of heterobimetallic photoCORMs and H_2O_2-mediated CO release from a water-soluble CORM. There are a myriad of reasons to use group 7 carbonyls; manganese is a favorable metal center to use as it is relatively Earth-abundant.[17] In particular, use of Re metal centers opens the possibility for luminescent photoactivity because of its accessible triplet MLCT state.[15,18,19]

A. Photochemical CO release from heterobimetallic Group 7 carbonyls

Photoactivated CORMs, or photoCORMs, are molecules capable of releasing CO upon stimulation by light.[20] A major issue in the practical application of photoCORMs is the high-energy light often needed to labilize the strong M-CO bond in inorganic systems[15]. The strong ligand field imparted by CO makes stimulation of a metal-to-CO ligand charge transfer or ligand field optical transition necessary for CO's direct photodissociation. These tend to take place at short wavelengths (< 400 nm). Many early photoCORMs are activated by wavelengths in the ultraviolet A (UVA) region, to which prolonged exposure has negative side effects.[21,22,23] To minimize these drawbacks, moving the wavelength of activation further into the red region of visible light of these inorganic photoCORMs is of interest. In particular, the near-infrared (NIR) region of the therapeutic window (approximately 750 nm to 1100 nm) is optimal for penetrating living tissue.[24,25]

One such method towards this end is utilizing the direct excitation of the metal-metal bond to ligand charge transfer (MMLCT) transition in a metal-metal bonded dinuclear carbonyl complex (in contrast to a metal to ligand charge transfer or MLCT). Previous studies in this group by Li et al., have proposed that homolytic cleavage of the Re-Mn bond in $(CO)_5ReMn(CO)_3L$ gives mononuclear metal radicals, which rapidly react to give species that highly favor dissociation of CO[26]. Upon photolysis at 659 nm, one such complex in which L = 1,10-phenanthroline was observed to release 2 equivalents of CO and to generate one equivalent of CO_2. These studies provide a "proof of concept" for this strategy of uncaging CO by

leveraging the metal-metal bond to ligand charge transfer (MMLCT) transition in a heterobimetallic complex such as illustrated in Figure 3.

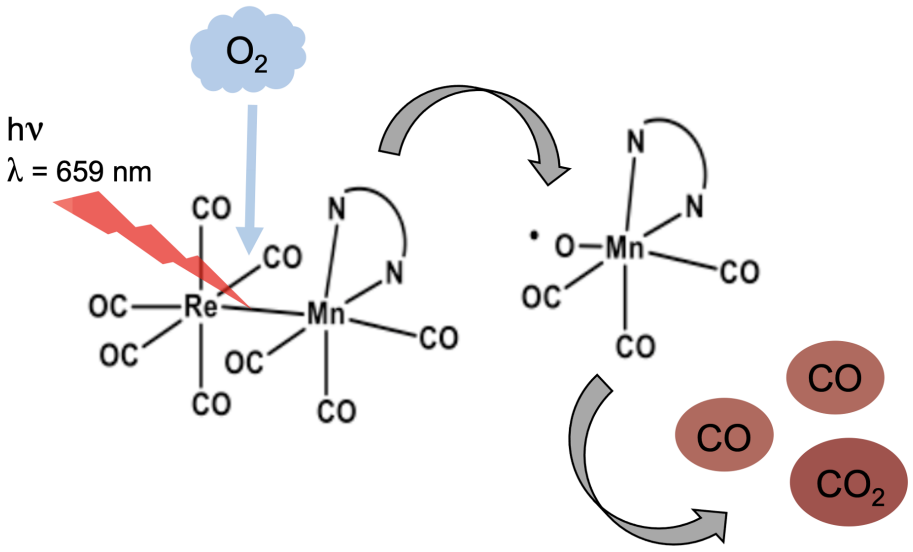

Figure 3. Proposed mechanism of CO and CO_2 release from $(CO)_5ReMn(CO)_3(phen)$, studied in this laboratory.[26]

The *fac*-$Re(CO)_3L$ fragment, in which L is a bidentate pyridine-based ligand, is well-known to exhibit a long-lived, luminescent ^{3}MLCT state. Indeed, Re-based photoCORMs have been previously reported, featuring polypyridyl ligands such as 2,2'-bipyridine, 1,10-phenanthroline, and 2-(2-pyridyl)-benzothiol.[15,18,19,27] More complex "antenna" ligands have shown to impart interesting properties to these Re(I) compounds for use as luminescent probes and other medicinal applications.[28]

To take advantage of the luminescent properties of the *fac*-$Re(CO)_3L$ fragment and extend the principle of long-wavelength photorelease of CO by leveraging the MMLCT optical transition, we propose conjugating this Re fragment containing the "antenna" ligand to a manganese pentacarbonyl moiety, thus combining the therapeutic potential of CO delivery and the trackability aspect of a luminescent molecule. Inspired by previous studies by Li, et. al. in this laboratory, we

endeavor to explore the reactivity, CO-releasing properties, and luminescence of these molecules with the general formula $(CO)_5MnRe(CO)_3(L)$, with ligands L referring to bidentate polypyridyl antenna ligands.[29]

Furthering strategies for long-wavelength-triggered release of SMBs can take inspiration from NO release; studies in this research group have explored using lanthanide upconverters such that NIR light is upconverted to visible light, which triggers NO release from a photoactivated NO-releasing molecule, or photoNORM.[30,32] Two-photon absorption (TPA) is another potential method for increasing the wavelength of photoCORM activation. Two-photon activity is nonlinear (dependent on light intensity) and involves successive absorption of photons, making long-wavelength activation more feasible.[33] Previous research in this group reported an aqueous-soluble manganese photoCORM featuring a two-photon-absorbing terpyridine ligand, allowing 800 nm NIR light to stimulate CO release under aerobic conditions.[25] Simultaneous TPE requires the use of high-intensity ultrafast lasers, meaning there is a strong incentive to develop alternative techniques for photomedicine. While the literature on two-photon absorbing photoCORMs is scant, inspiration can be taken from the numerous applications of TPA in medicinal settings.[34]

B. H_2O_2 mediated CO release from CORMs

Outside of photoactivation, a few strategies for targeting internal CO release are particularly noteworthy. Potential triggers for CO release can consist of ambiently available physiological molecules such as H_2O_2 or O_2.[35] Chemical

activation of CORMs is viable when the activator is a species overexpressed in areas needing treatment with CO. For example, endogenous hydrogen peroxide and other reactive oxygen species are overexpressed in tumor cells and play diverse roles in tumor growth.[36,37] This strategy of targeting particular species present in tumors has been used to great effect by Podgorski, Turro, and Kodanko in photo-releasing cysteine protease inhibitors using Group 8 polypyridyl complexes. These therapies specifically target cathepsin K, a cysteine cathepsin overexpressed in many cancers.[13,38,39,40,41] Another example of bioaccumulation of anticancer agents based on affinity for particular targets in tumoral areas is Ru-caged CHS-828 (N-(6-(4-chlorophenoxy)hexyl)-N'-cyano-N''-4-pyridylguanidine), which is a drug that has completed Phase I clinical trials against solid tumors. CHS-828 is a nicotinamide phosphoribosyltransferase (NAMPT) inhibitor, NAMPT being a crucial protein in the reproduction of cancer cells.[42] Wei and Renfrew investigated the anticancer action of CHS-828 coordinated to Ru(tpy)(bpy) and Ru(tpy)(biq); they observed both complexes selectively accumulate in the mitochondria of tumor cells.

While H_2O_2-mediated treatments of tumors have been investigated,[43,44] few studies have been conducted on the mechanism of CO release from inorganic CORMs upon their reactions with H_2O_2. In particular, the CORM studied in this group previously, $Mn(CO)_3Br(4,4'\text{-bpy-}(COOH)_2)$, is of interest because its ionizable carboxylic acid moieties increase the water-solubility of the molecule (Figure 4).[45] This would increase its biocompatibility, a trait favorable in CO-releasing therapy.

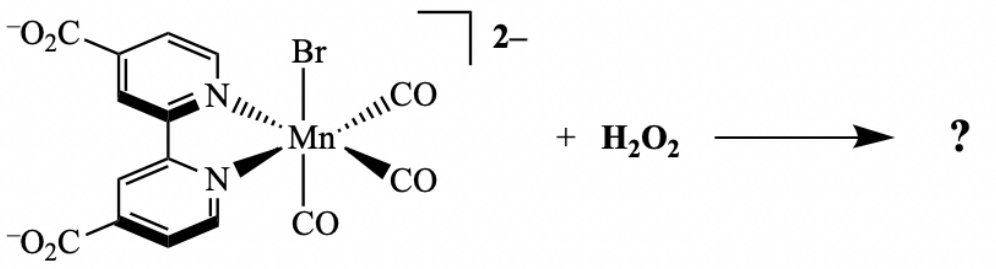

Figure 4. Reaction of Mn(I) tricarbonyl complex studied by Barrett, et. al. with hydrogen peroxide.[43]

Kinetics experiments performed by reacting the CORM in question with H_2O_2 under various conditions revealed the rate-determining step to be first order with respect to each reactant. The authors posit that the rate determining step could potentially be outer-sphere electron transfer, an inner-sphere substitution process, or attack on a CO ligand by the hydroperoxy anion (HOO^-, the conjugate base of H_2O_2). A higher rate of reaction was also observed upon increasing the pH of the buffer solution, suggesting that the hydroperoxy anion is more reactive with the CORM than H_2O_2 itself; this lends credence to the substitution and CO attack as probable mechanisms of the rate-determining step.

Barrett, et. al. note that the CORM under study is itself photoactive; there may be potential for synergistic chemical and photoactivated CO release, or coupling of these with another therapeutic mode. Previous studies into H_2O_2 triggered CO release note that drug release coupled with photothermal therapy increases the cytotoxicity at tumor sites.[46] Photothermal therapy is a technique by which light activation results in an increase in temperature, leading to cell-killing action in the targeted area. This strategy of combining H_2O_2-activated CO release and photothermal therapy has recently been explored by Ma and coworkers.[47]

C. Proposed research

My research has been divided into two projects. The first investigates labilizing the Re-Mn bond in heterobimetallic complexes with the general formula $(CO)_5MnRe(CO)_3L$, in which L is a bipyridine or similar unsaturated ligand with low-lying π* orbitals. We hypothesize that a $Re(CO)_3L$ fragment conjugated to a manganese pentacarbonyl will yield a “theranostic” photoCORM, where upon photoreaction, the manganese fragment releases CO and the product of the Re fragment is photoluminescent. The photochemical properties of the dimer of Re(CO)(bpy) are also discussed in the course of this investigation; while CO release is not expected from $[Re(CO)_3bpy]_2$, its anticipated luminescent properties and photochemical behavior of its metal-metal bond are expected to be similar to the heterobinuclear compounds of study.

The second project is regarding the mechanism of CO release from the H_2O_2 activated CORM previously studied by Barrett, et. al. by investigating the model compound $[Mn(CO)_4bpy\text{-}(COOH)_2][SbF_6]$.This complex features an additional CO ligand in the place of bromide of the Barrett compound. We hypothesize that this substitution will eliminate the mechanistic possibility of reaction with H_2O_2 that involves substitution of the bromide ligand, allowing further insight into the interaction between H_2O_2 and this class of CORMs. The synthesis and characterization of $[Mn(CO)_4bpy\text{-}(COOH)_2][SbF_6]$ are detailed herein.

II. Heterobimetallic photoCORMs

A. Background

Photoactivated CO release for medical applications has been under study for a little over 2 decades. The first CORMs activated by light stimulation were Mn_2CO_{10} and $Fe(CO)_5$, reported in 2002 by Motterlini and coworkers. Myoglobin assays demonstrated these low-valent, first-row transition metal carbonyls converted Mb to MbCO upon activation by a broad-spectrum, cold light source.[48] As research into photoCORMs advanced, particular design principles arose to achieve the goals of using photoCORMs in medical contexts. One particular issue of early photoCORMs, which endures, is the necessity of short wavelength light to photodissociate CO or otherwise release CO from the transition metal complex. Standards for useful photoCORMs are biocompatibility (low toxicity, stability in physiological conditions); dark-stability, as well as thermal and chemical inertness (that is, the compound does not react until stimulated by light).[49]

While organic photoCORMs are an area under study, behavior of ligand metal carbonyl complexes is better understood. Some examples are covalently bonded CO release from ketones and similar compounds featuring carbonyls that act as organic photoCORMs.[50,51,52] However, organic photoCORMs do have some advantages over inorganics; namely, many are easily functionalizable and may be easier to synthesize compared to some metal complexes.[53] In fact, some design principles of organic photoCORMs can be applied to the design of inorganic photoCORMs; indeed, many organic photoCORMs exhibit long-lived fluorescence

due to the presence of conjugated electronic systems. Building inorganic photoCORMs featuring similar systems could add fluorescence and a way to track photoCORMs as they act.

Heavier transition metal carbonyls such as those featuring tungsten, ruthenium, and rhenium are also part of the pantheon of inorganic photoCORMs. In particular, the term “photoCORM” was coined to describe a tungsten-based carbonyl from this group[20]; Re-based photoCORMs have also been investigated by this group in the past.[15] Notably, the use of second- and third-row transition metals introduces large spin-orbit coupling interactions into the photochemistry of these complexes. Activation of the MLCT transitions has led to photoluminescent photoCORMs, leading to fluorescence concomitant with CO release.[18] Adding this property to photoCORMs would establish theranostic complexes that combine the diagnostic effects of fluorescent action and therapeutic effects of CO release. A particular method of building theranostic photoCORMs, explored by Li, et. al. in 2017, is conjugation of metal centers within inorganic photoCORMs. In this chapter, we propose conjugating a rhenium carbonyl fragment containing an “antenna” ligand to a manganese pentacarbonyl moiety. We endeavor to explore the reactivity and luminescence of these molecules with the general formula $(CO)_5MnRe(CO)_3L$, with ligands L referring to bidentate polypyridyl ligands.

While work continues apace with improving inorganic photoCORMs, many issues must be resolved. Out of many established inorganic photoCORMs, there are major questions about biocompatibility and therapeutic effects of photoCORMs outside of direct CO release. Additional *in vitro* studies, examining cytotoxicity, and

anti-inflammatory assays are rare in studies of photoCORMs, and a more holistic appraisals are needed to expand the portfolio of functional photoCORMs.[54,55]

B. Experimental

Materials. Bromopentacarbonylmanganese(I) (98%), dirhenium decacarbonyl (98%), and anhydrous 5-chloro-1,10-phenanthroline, 5-bromo-1,10-phenanthroline, and 5,5'-dicarboxyl-1,10-phenanthroline were purchased from Strem Chemicals and used without further purification. 2,2'-bipyridine and 2-chloroethanol were purchased from Sigma-Aldrich Chemical Company and used without further purification. 1,10-phenanthroline monohydrate was purchased from Strem Chemicals and dried for 30 minutes at 120^{o}C in a vacuum oven prior to use. Dichloromethane, diethyl ether, toluene, n-hexane, and n-pentane were purchased from Fisher Scientific and used without further purification. Tetrahydrofuran was dispensed from a solvent system equipped with an activated alumina column and stored over 3Å molecular sieves under an argon atmosphere.

Analytical Instrumentation. Solution optical absorption spectra were recorded in 1.0-cm-path-length quartz cells using a Shimadzu dual beam UV-2401 PC and StellarNet SL5-DH spectrophotometers. Solution NMR spectra were also recorded on a 500 mHz Varian Unity Inova Spectrometer using a 5 mm Broadband Probe with pulsed field gradients. Photoluminescence was measured using a PTI fluorimeter. Solid-state crystal structures were determined by X-ray diffraction on a Kappa Apex II single-crystal diffractometer. Photolyses were carried out on solutions in a custom-made Schlenk cuvette consisting of quartz cuvette fused to glass tubing and

stopcocks designed for attachment to a vacuum line and for degassing, introducing or withdrawing gas samples.[9] Solutions for anaerobic experiments were degassed by freeze−pump−thaw (3x) procedures, after which the Schlenk cuvette was backfilled with purified argon.

Quantum yield (Φ) measurements followed the procedure described by Li et al.[21] Plots of molecules reacted ($N_{reacted}$) calculated from absorption changes vs photons absorbed (N_{abs}) calculated from the incident photon. Φ values were determined from the slopes of the $N_{reacted}$ versus N_{abs} plots and were corrected for any dark reactions.

Syntheses of $Re(CO)_3(L)Cl$

***fac*-[$Re(CO)_3$(bpy)Cl]:** This was prepared by a modified literature procedure.[56] Dirhenium decacarbonyl (1.000 g, 1.53 mmol) was refluxed with 2,2'-bipyridine (0.716 g, 4.59 mmol) in 2-chloroethanol (120 mL) for 18 hours under Ar atmosphere. After 18 h, the reaction solution was vacuum dried and dissolved in 50 mL of dichloromethane (DCM) and washed with water (50 mL × 3). A yellow solid was obtained after evaporating the DCM and the solid was dried in vacuum oven at 60 C° for 12 h and washed with hexanes. Total yield was 1.085 g (76.8%). ^{1}H NMR (500 MHz, CD_2Cl_2, ppm) δ = 9.04 (d, 2H), 8.23 (d, 2H), 8.12 (t, 2H), 7.58 (m, 2H). NMR spectra are recorded in the Appendix.

***fac*-[$Re(CO)_3$(phen)Cl]:** Dirheninum decacarbonyl (0.7233 g, 1.108 mmol) was refluxed with 1,10-phenanthroline (0.5743 g, 2.897 mol) in 2-chloroethanol (50 mL) for 18 h under an Ar atmosphere. The reaction mixture was cooled to room

temperature, dried, dissolved in DCM and washed with water three times, then dried. A yellow-orange solid was obtained after washing the solid with hexanes. Total yield was 0.3585g (33%). ^{1}H NMR (500 MHz, CD_2Cl_2), δ = 9.38 (d, 2H), 8.61 (d, 2H), 8.07 (d, 2H), 7.91 (d, 2H) ppm.

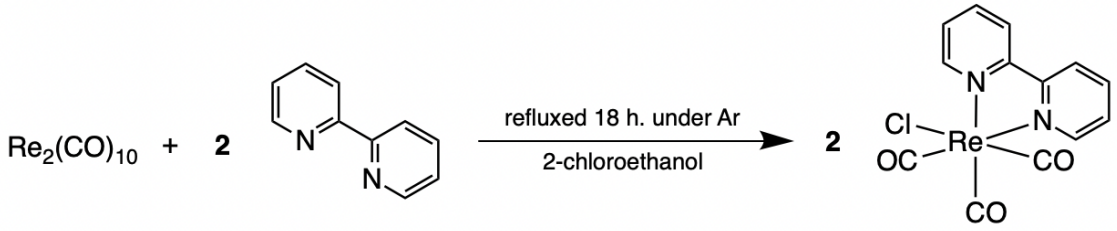

Figure 5. General synthetic scheme to form $Re(CO)_3(L)Cl$ from $Re_2(CO)_{10}$.

$Re(CO)_5Cl$ was synthesized according to a literature procedure.[30] Dirhenium decarbonyl (1.3176 g, 2.0192 mmol) was dissolved in DCM. Iodobenzene dichloride ($PhICl_2$) was prepared according to a literature procedure.[31] Dry $PhICl_2$ (0.5900 g, 2.108 mmol) was added to the solution and stirred in the dark for 6 hours under atmospheric conditions. The pink-and-white suspension was filtered and washed with hexanes and pentanes. A white powder was recovered. Total yield was 1.3092 g (89.6%). The solid was used as a source of rhenium pentacarbonyl without further characterization.

fac-[$Re(CO)_3$(5-phen-Br)Cl] (phen-Br = 5-bromo-1,10-phenanthroline). $Re(CO)_5Cl$ (0.2011 g, 0.5560 mmol) was dissolved in hot toluene (150 mL) and refluxed with phen-Br (0.1518 g, 0.5858 mmol) for 3 hours under ambient conditions. The reaction mixture was cooled to 0°C and filtered and washed with cold toluene and hexanes to yield a yellow powder. Yield: 0.2467 g, 77%.

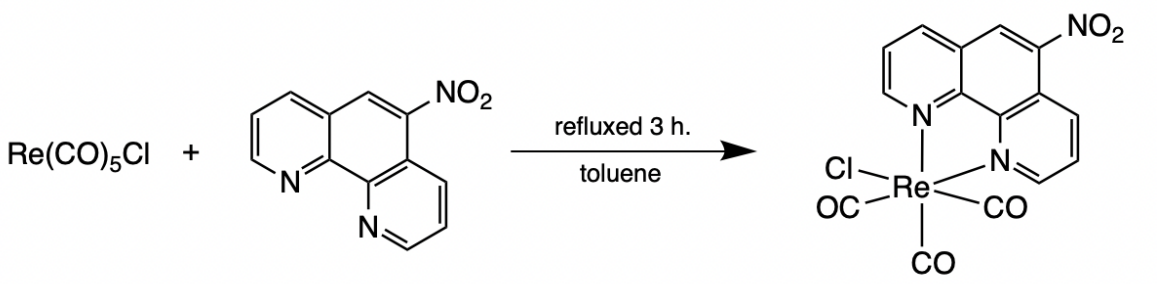

Figure 6. General synthetic scheme to form $Re(CO)_3(L)Cl$ from $Re(CO)_5Cl$.

5-nitro-1,10-phenanthroline (phen-NO_2) was synthesized according to a modified literature procedure.[57] 60 mL of concentrated sulfuric acid was heated to 80˚C in a 3-necked round-bottomed flask outfitted with a reflux condenser. 6.222 g (31.39 mmol) of 1,10-phenanthroline monohydrate was added to the concentrated H_2SO_4, which turned yellow. The solution was heated to 140˚C and 20 mL concentrated HNO_3 was added carefully in 1 mL portions over 2 hours. Orange nitrous gases and white sulfurous gases were evolved from the solution upon addition of each portion of acid. The reaction mixture was carefully refluxed for 3 hours at 170˚C. Then, the mixture was heated overnight at 100˚C for all gases to finish evolving. The orange-yellow solution was mixed with approximately 200 g (1 tray) of DI ice cubes. The solution was transferred to a 2 L round-bottomed flask; 1 L of 30% NaOH, with an additional 60 g of NaOH, was added to the flask to make it basic to litmus. The solution turned dark grey and a large quantity of precipitate formed. The solution was neutralized to litmus using 300 mL of dilute (0.3 M) HNO_3, then vacuum filtered. The gray solid was dried in a vacuum oven at 60°C overnight and stored in a desiccator, yielding 4.2854 g (60.61%). ^{1}H NMR (500 MHz, $CDCl_3$), δ = 9.33 (m, 2H), 9.02 (d, 1H), 8.70 (s, 1H), 8.44 (d, 1H), 7.82 (m, 2H) ppm.

***fac*-[Re(CO)$_3$(phen-NO$_2$)Cl].** $Re(CO)_5Cl$ (0.2089 g, 0.5775 mmol) was dissolved in hot toluene (150 mL) and refluxed with phen-NO_2 (0.1554 g, 0.6900 mmol) for 3 hours under ambient conditions. The orange reaction mixture was cooled to 0^{o}C and concentrated to 40 mL using a rotary evaporator. The solution was filtered and washed with cold toluene and hexanes to yield a yellow powder. Yield: 0.2997 g, 97%. ^{1}H NMR (500 MHz, CD_2Cl_2), δ = 9.52 (m, 2H), 9.36 (d, 1H), 8.99 (s, 1H), 9.79 (d, 1H), 8.06 (m, 2H) ppm.

***fac*-Re(CO)$_3$(5,5'-bpy-(COOH)$_2$)Cl** (5,5'-bpy-$(COOH)_2$ = 2,2'-bipyridine-5,5'-dicarboxylic acid) was prepared by a procedure analogous to that used to prepare *fac*-[$Re(CO)_3$(phen-NO_2)Cl] using 0.1565 g $Re(CO)_5Cl$ and 0.1281 g 5,5'-bpy-$(COOH)_2$. Yield: 65.9 mg, 27.6%.

Syntheses of (CO)$_5$MnRe(CO)$_3$(L)

(CO)$_5$MnRe(CO)$_3$(bpy): The intermediate Na[$Re(CO)_3$(bpy)] was first prepared as follows: Hg(Na) (3%) (2.4 g) was added to a dry round bottom flask containing ~30 mL dry THF under an argon atmosphere. Under flowing argon, solid $Re(CO)_3$(bpy)Cl (0.150 g, 0.324 mmol) was added to this solution, and the mixture was stirred for 3 h in dark. The initially yellow $Re(CO)_3$(bpy)Cl solution underwent a change to the dark green of Na[$Re(CO)_3$(bpy)]. The Na[$Re(CO)_3$(bpy)] was not isolated; instead the THF solution was kept under an argon atmosphere until being used in its entirety during the same day in each synthetic procedure.

A THF solution containing the rhenium anion Na[$Re(CO)_3$(bpy)] (0.324 mmol) was carefully transferred via cannula to another round bottom flask containing

$Mn(CO)_5Br$ (0.100 g, 0.365 mmol) dissolved in 35 mL of dry THF. The solution was then allowed to stir under argon at 40°C, with the exclusion of light for 12 h. The mixed solution color changed from a yellow color to orange. After 12 h, the solvent was removed under vacuum, and the resulting solid was purified by flash chromatography over activated alumina. The column was washed with one column volume of pure hexanes, then it was eluted with a gradient of DCM/hexanes (0%-50% DCM). The main component from the column chromatography purification was collected giving a final product with a yield of 43 mg (15%).

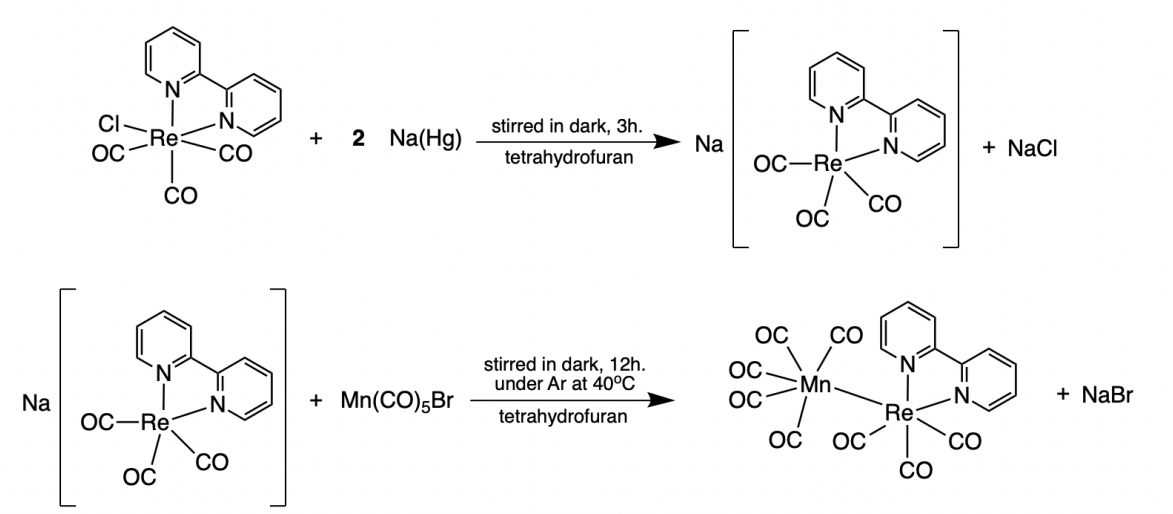

Figure 7. General synthetic scheme to form $(CO)_5MnRe(CO)_3(L)$.

$CO_5MnRe(CO)_3$(phen) was prepared according to a similar procedure as other $(CO)_5MnRe(CO)_3$bpy compounds. 0.2472 g (0.5087 mmol) of $Re(CO)_3$(phen)Cl was added to 30 mL of THF with excess sodium amalgam. The solution was stirred under Ar atmosphere in the dark for 3 hours, then air-free syringe transferred to a flask containing a solution of 0.1286 g (0.4678 mmol) $Mn(CO)_5Br$ dissolved in 20 mL of THF. This solution was stirred in the dark in an Ar-

atmosphere glove box for 12 hours at 55°C. The solution was filtered through a glass pipette using a Kimwipe and activated alumina, then dried and purified by flash chromatography over activated alumina. The column was washed with one column volume of pure hexanes, then it was eluted with a gradient of DCM/hexanes (0%-50% DCM). Not enough product was collected to report a yield.

[$(CO)_5$Mn–Re$(CO)_3$(phen-Br)Cl] was prepared according to a similar procedure as other $(CO)_5MnRe(CO)_3(L)$ complexes. 0.2045 g fac-[$Re(CO)_3$(phen-Br)Cl] was added to 30 mL of dry, degassed THF along with excess sodium under an argon atmosphere. The solution was stirred in the dark for 3 hours, then syringe-transferred to a flask with a solution of 0.1103 g $Mn(CO)_5Br$ dissolved in 20 mL of dry, degassed THF. The reaction mixture was stirred overnight at 40°C; the dark green reaction mixture slowly turned orange. Yield: 3.2 mg, 1.22%.

Synthesis of $[Re(CO)_3(bpy)]_2$

3% Hg(Na) (0.8956 g) was added to a vial containing THF. A yellow THF solution of $Re(CO)_3(bpy)Cl$ (0.0443 g, 0.0959 mmol) was added to the Hg(Na). Almost immediately, the color changed from yellow to dark, murky green. This is consistent with Dr. Li's observations of the $Na[Re(CO)_3(bpy)]$ anion.

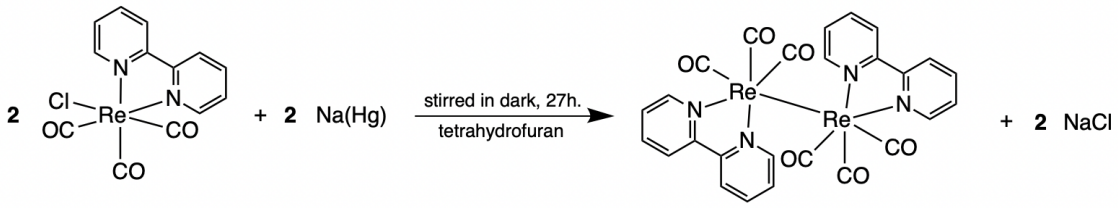

Figure 8. General synthetic scheme to form $[Re(CO)_3(bpy)]_2$.

After 3 hours, the vial containing the Na[$Re(CO)_3$(bpy)] reaction mixture was moved to another nitrogen-atmosphere glovebox. Solid $Mn(CO)_5Br$ was weighed (0.028 g, 0.10 mmol) and dissolved in THF to form a bright orange solution. When the vial of Na[$Re(CO)_3$(bpy)] solution was opened, it was dark purple in color; the solution was then pipetted into the $Mn(CO)_5Br$ solution. The reaction mixture was stirred for 24 hours at 50°C and was a dark yellow color. After 4 additional hours of heating at 100°C, the solution turned a darker orange color. The crude solution was then stored in a freezer at –1.1°C.

The crude reaction mixture was dried under vacuum. The resulting dark, wine-colored solid was washed with hexane and a clear, violet-colored fraction was extracted and filtered. The remaining solid was dissolved in DCM and divided into two volumes; one was layered with hexanes and the other in a reverse vapor diffusion setup with hexanes. These three solutions were stored in a freezer at –1.1°C to encourage crystallization. From layering and vapor diffusion crystallizations, small, purple-red crystals were observed and collected for XRD analysis.

C. Results and Discussion

Synthesis and Characterization

Described herein is a series of *fac*-$Re(CO)_3$(L)Cl complexes and initial explorations of $(CO)_5MnRe(CO)_3L$ complexes, including UV-Visible and luminescence studies. Out of the handful of $Re(CO)_3LCl$ complexes examined, the complex featuring L= 1,10-phenanthroline showed the highest MLCT absorptivity of

each complex; it also showed the most intense photoluminescence upon excitation at 400 nm.

The variety in absorptivity and luminescence among these *fac*-$Re(CO)_3(L)Cl$ complexes illustrates how ligand design can tune the properties of inorganic photoCORMs. Interestingly, negligible luminescence was seen from $Re(CO)_3$(phen-$NO_{2)}Cl$ complexes. While its MLCT is at a slightly longer wavelength (400.5 nm) compared to the un-functionalized phenanthroline analogue (387.5 nm), the addition of low-lying π-acceptor orbitals from the $-NO_2$ group is the likely culprit for deactivating the typically luminescent ^{3}MLCT decay. The other $Re(CO)_3(L)Cl$ complexes, especially L = 5,5'-bpy-$(COOH)_2$, could themselves be investigated for CO release with some structural modifications; for example, swapping the Cl ligand for a water-soluble moiety or H_2O could increase aqueous solubility to make these viable photoCORMs in their own right.[15,19]

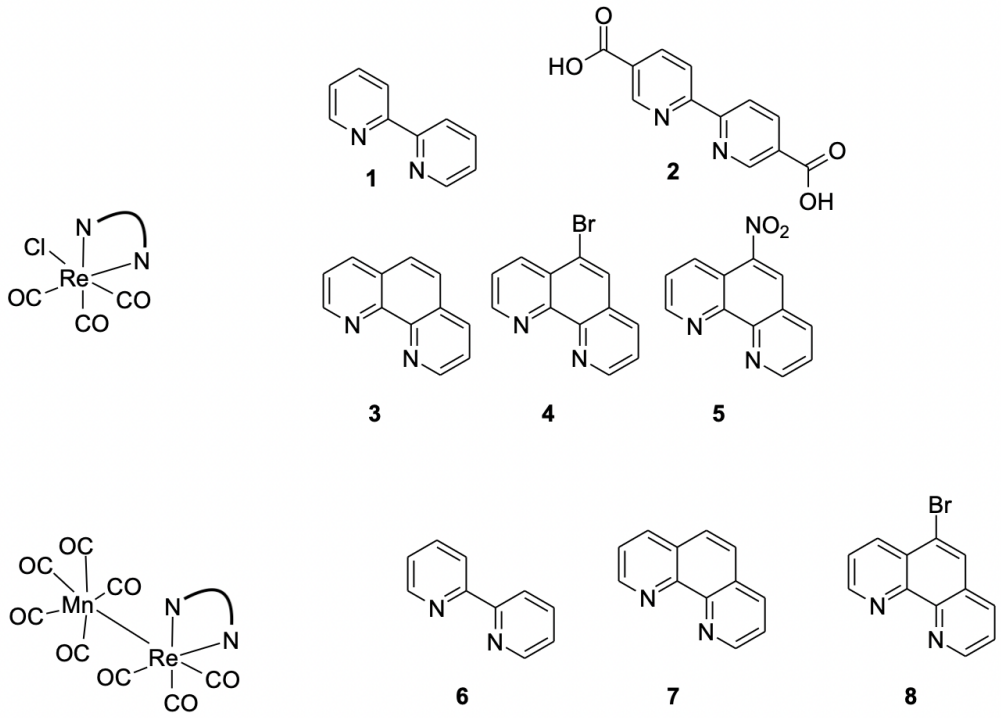

Figure 9. Structures of compounds examined in this paper. 1 = *fac*-$Re(CO)_3(bpy)Cl$, 2 = *fac*-$Re(CO)_3(5,5'\text{-bpy-}(COOH)_2)Cl$, 3 = *fac*-$Re(CO)_3(phen)Cl$, 4 = *fac*-$Re(CO)_3(5\text{-phen-Br})Cl$, 5 = *fac*-$Re(CO)_3(phen\text{-}NO_2)Cl$, 6 = $(CO)_5MnRe(CO)_3(bpy)$, 7 = $(CO)_5MnRe(CO)_3(phen)$, 8 = $(CO)_5MnRe(CO)_3(5\text{-phen-Br})$.

Complexes $(CO)_5MnRe(CO)_3L$ were also examined in which L = 2,2'-bipyridine and 1,10-phenanthroline. The syntheses described followed procedures outlined by Morse and Wrighton[22] and extended by Li, et. al.[21] for the synthesis of similar complexes. The optical absorption spectra of **6** and **7** in CH_3CN solution showed MMLCT bands at 500 and 550 nm.

These bimetallic complexes are sensitive to light and subject to decomposition upon irradiation. $[(CO)_5MnRe(CO)_3(L)]$ and their precursors *fac*-$[Re(CO)_3(L)Cl]$ were characterized by ^1H NMR spectrometry and UV-visible spectroscopy. Lots of work needs to be done to refine these syntheses, the author unable to replicate results from Li's thesis such as collecting a pure, crystalline

sample of any [$(CO)_5MnRe(CO)_3(L)$] compound. The UV-visible spectrum of [$(CO)_5MnRe(CO)_3(bpy)$] in aerobic acetonitrile (MeCN) solution displays an absorption band at 500 nm which is attributed to a MMLCT ($\sigma^{MM} \rightarrow \pi^{L*}$) transition in analogy to earlier studies with related complexes.[22]

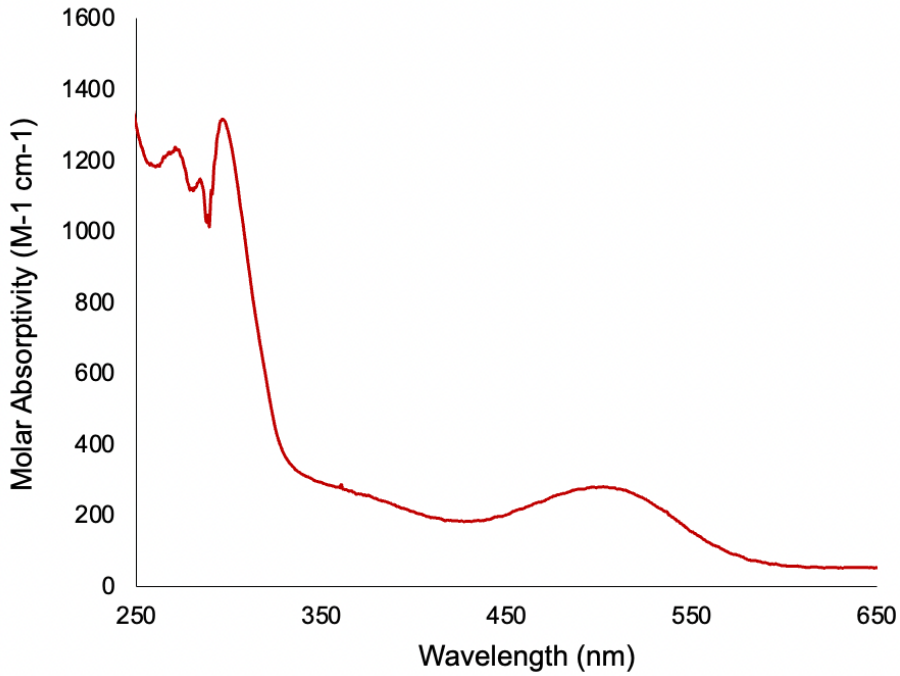

Figure 10. UV-Visible spectrum of putative $(CO)_5MnRe(CO)_3bpy$ (5.30×10^{-4} M, THF). λ_{max}(MMLCT) = 502 nm (281 M^{-1} cm^{-1})

Upon increasing the conjugation of the chromophore ligand from bpy to phen, the MMLCT band shifts to the red, corresponding to the decrease in LUMO energy. While these show trailing absorbances into longer wavelengths, more work must be done to extend wavelength of activations of these photoCORMs into phototherapeutic window.

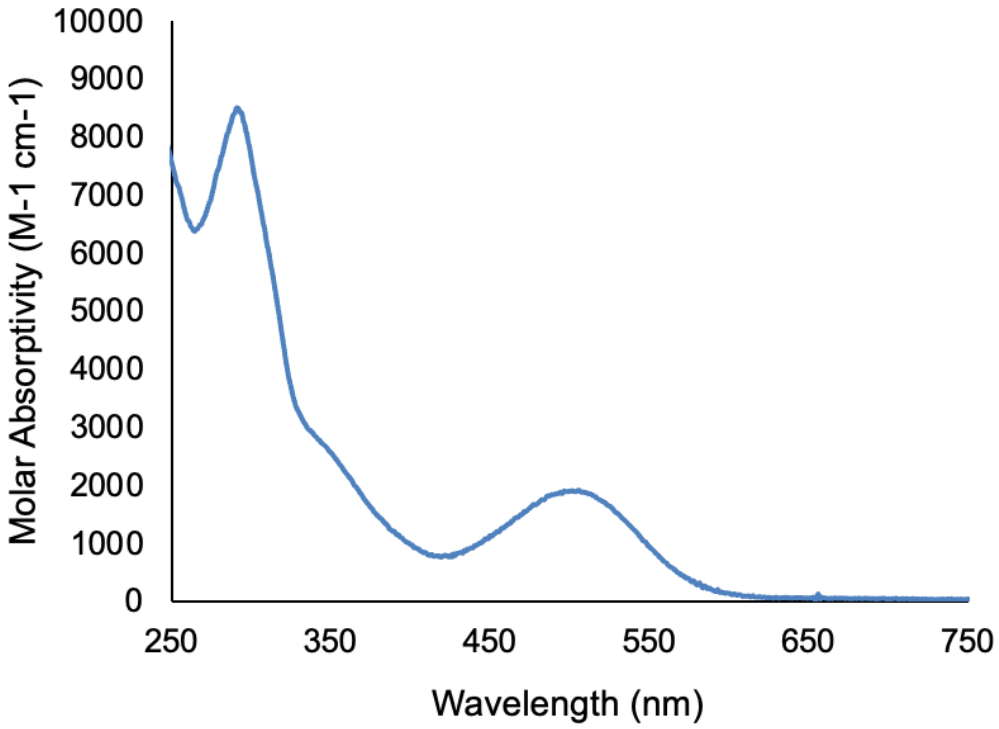

Figure 11. UV-Visible spectrum of $[Re(CO)_3bpy]_2$ (1.76×10^{-4} M, CH_3CN).
λ_{max}(MMLCT) = 505 nm (1910 M^{-1} cm^{-1})

The dimeric complex $[Re(CO)_3bpy]_2$ (**9**) was formed was formed when the $[Re(CO)_3bpy]^-$ anion was oxidized in presence of air. While it is not expected to release CO, its luminescent properties could make it an interesting compound for diagnostic use and provide insight into the activation of metal-metal bonds in binuclear photoCORMs. This complex shows an MMLCT band centered around 500 nm (Figure 11). Single crystals of **9** were grown and analyzed using X-ray diffraction to yield a solid-state structure (Figure 12).

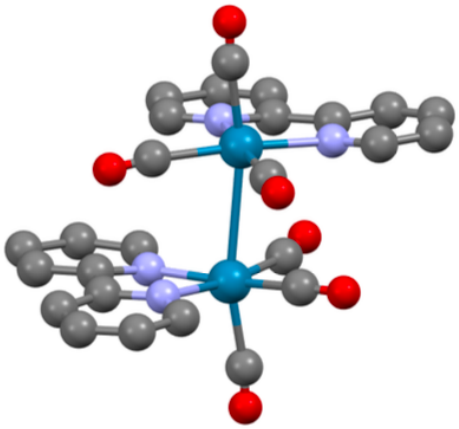

Figure 12. Rendering of *fac*-[Re(CO)$_3$(bpy)]$_2$ crystal structure in Mercury. Teal = Re; lavender = N; gray = C; red = O. Hydrogen atoms are omitted for clarity.

Photochemical Studies

The binuclear complexes **6-8** are stable in the dark both in the solid and in solution, but they are photo-sensitive. The MMLCT bands (λ_{max} = 480-505nm) of these complexes in CH_3CN solution tail to longer wavelengths and are photoactive when excited using a green light emitting diode (LED) operating at 536 nm. While the complex **6** synthesized by the author was not isolated, Figure 7 shows the steady decrease of the MMLCT band of complex **6** in aerobic CH_3CN when irradiated at 536 nm.

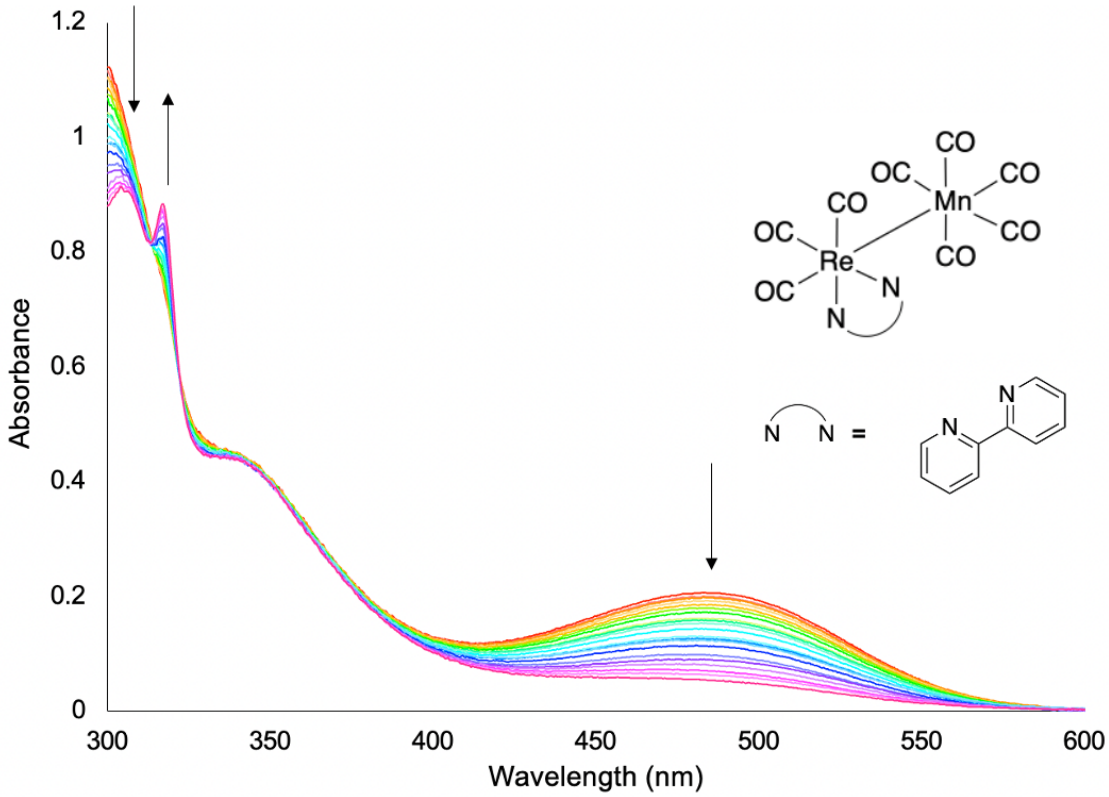

Figure 13. Changes in electronic absorbance spectrum of $[(CO)_5MnRe(CO)_3(bpy)]$ (4.3×10^{-4} M in aerobic CH_3CN) upon continuous photolysis by a 536 nm, 24 mW LED source.

Upon continuous irradiation at 536 nm in aerobic acetonitrile, $[(CO)_5MnRe(CO)_3(L)]$ saw a decrease in its MMLCT, but higher-energy bands remained, indicating that the photoproducts can access an MLCT transition. Since $[(CO)_5MnRe(CO)_3(bpy)]$ contains a rhenium tricarbonyl moiety, it is possible that $[(CO)_5MnRe(CO)_3(bpy)]$ or/and its photoproducts could be emissive at room temperature. Previous studies found that this compound in acetonitrile solution has a very low emission intensity with λ_{max} = 555 nm, but the intensity of luminescence increased after the compound was exhaustively photolyzed (Figure 14).

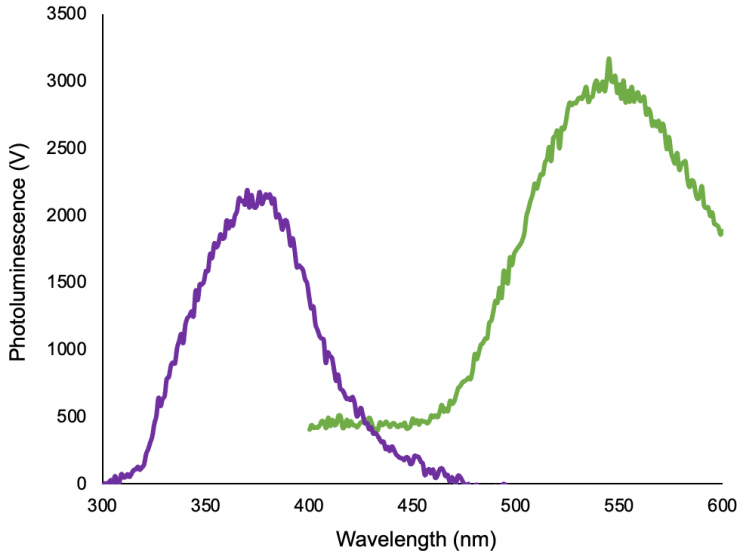

Figure 14. Photoluminescence of an exhaustively photolyzed sample of $[(CO)_5MnRe(CO)_3(bpy)]$ (4.3 x 10^{-4} M in aerobic CH_3CN) upon excitation at 380 nm (green) and emission at 550 nm (violet).

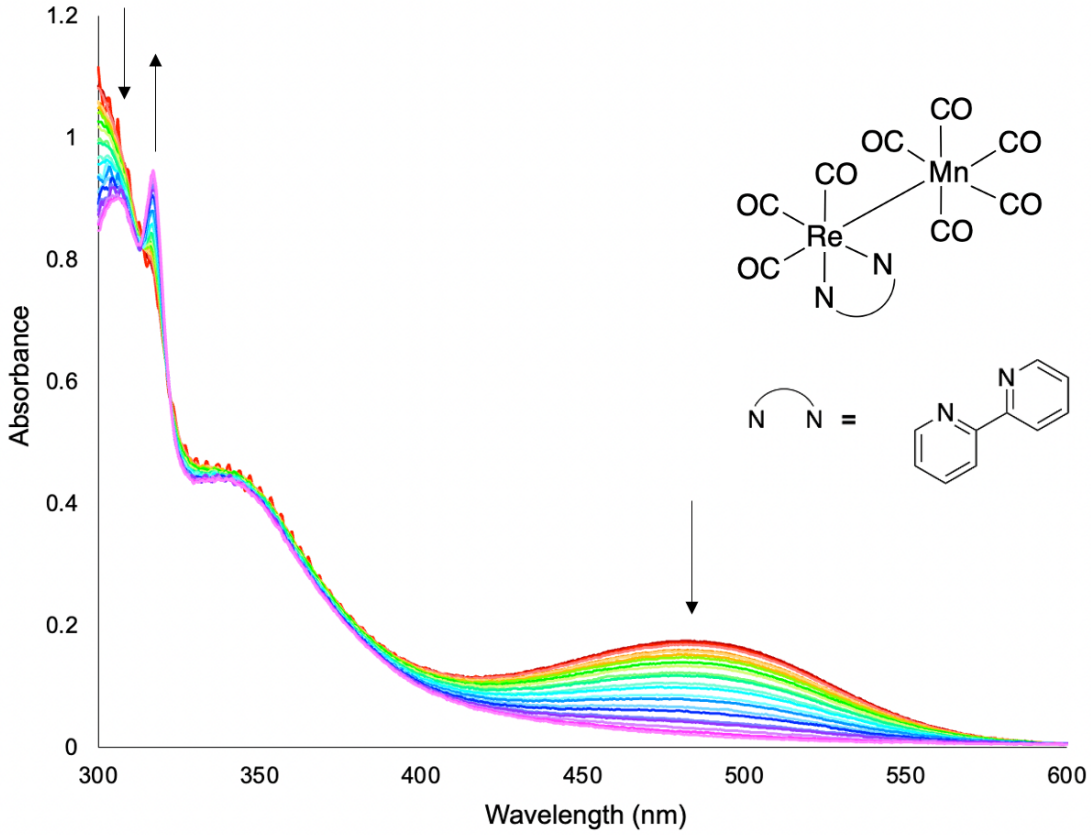

Figure 15. Changes in electronic absorbance spectrum of $[(CO)_5MnRe(CO)_3(bpy)]$ (4.3 x 10^{-4} M in deaerated CH_3CN) upon continuous photolysis by a 536 nm, 24 mW LED source.

The same experiment was repeated with a deaerated acetonitrile solution using freeze-pump-thaw. In contrast to the aerated solution, the deaerated solution had to be irradiated for much longer to see a comparable decrease in the MMLCT. This suggests that the presence of oxygen affects the photolysis reaction, following Li's studies of the same compound.[22] The respective quantum yields were 0.368 and 0.302 for the photoreaction in the presence of and the absence of oxygen, respectively. (Figure 9).

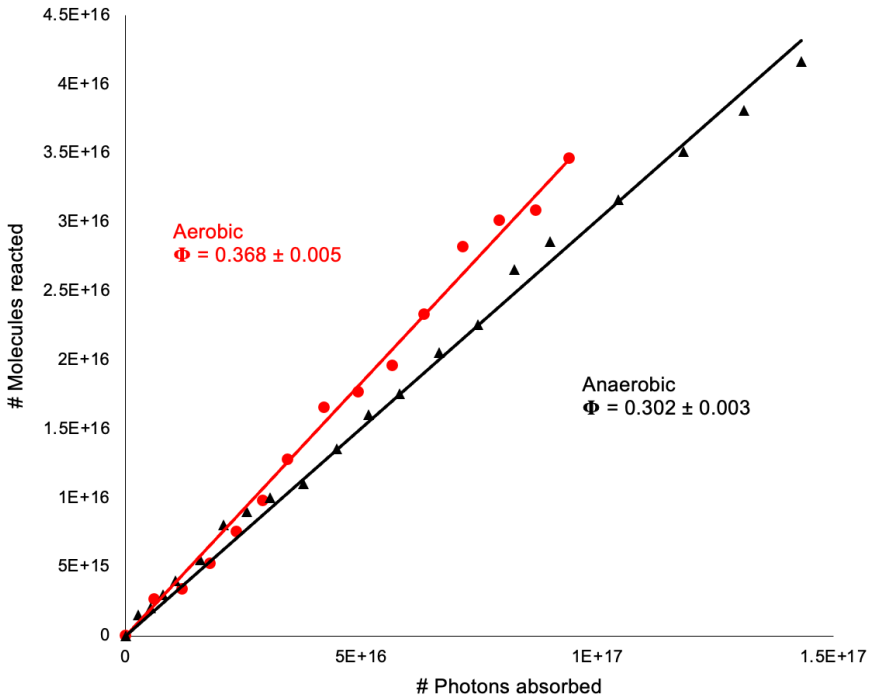

Figure 16. Comparison of results for quantum yields of 50% photobleaching of MMLCT present in both aerated and deaerated CH_3CN solutions of $(CO)_5MnRe(CO)_3bpy$ using a 536 nm LED.

Figure 16 illustrates the modest difference between quantum yields of photoreaction of $(CO)_5MnRe(CO)_3bpy$ in aerobic and anaerobic media (acetonitrile)

upon 50% depletion of the MMLCT. While there was a modest difference the Φ values between aerobic and anaerobic conditions, it should be noted that fewer data points were collected for the complex's reaction in air to reach 50% bleaching of the MMLCT. Further studies are needed to confirm these results; while they are similar to those reached by Li, et al. in 2017, the lower purity of the sample used for analysis complicates the results.[29]

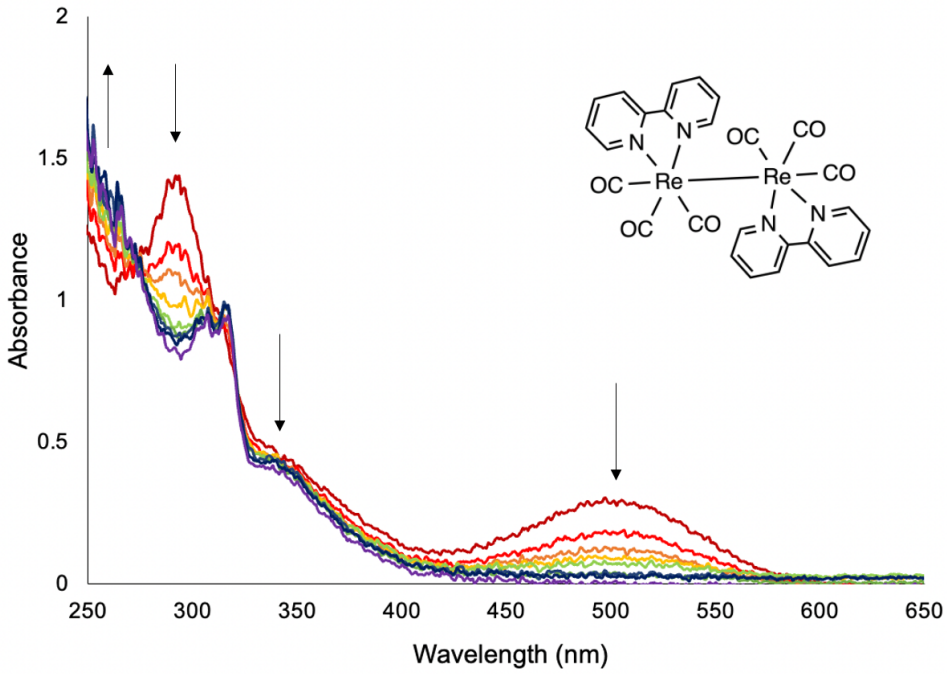

Figure 17. Changes in electronic absorbance spectrum of $[Re(CO)_3(bpy)]_2$ (1.76×10^{-4} M in aerobic CH_3CN) upon continuous photolysis by a 536 nm, 24 mW LED source.

The depletion of the MMLCT band in $[Re(CO)_3bpy]_2$ was also investigated using the same 536 nm green LED. The UV-Visible spectrometer used was a lower-resolution instrument, but a decrease in the MMLCT can still be seen at 505 nm. The related quantum yield calculations show a slope of greater than 1, indicating that

more photoreactions are taking place than the amount of light being absorbed by this complex in solution. While this observation requires further investigation to confirm, it suggests potential chain reaction induced by photoreactions to give $Re(CO)_3$bpy radicals followed by subsequent reaction of these $Re(CO)_3$bpy radicals with dimer molecules. This would show an increased number of metal-metal bond breaking interactions despite a static amount of light entering the solution.

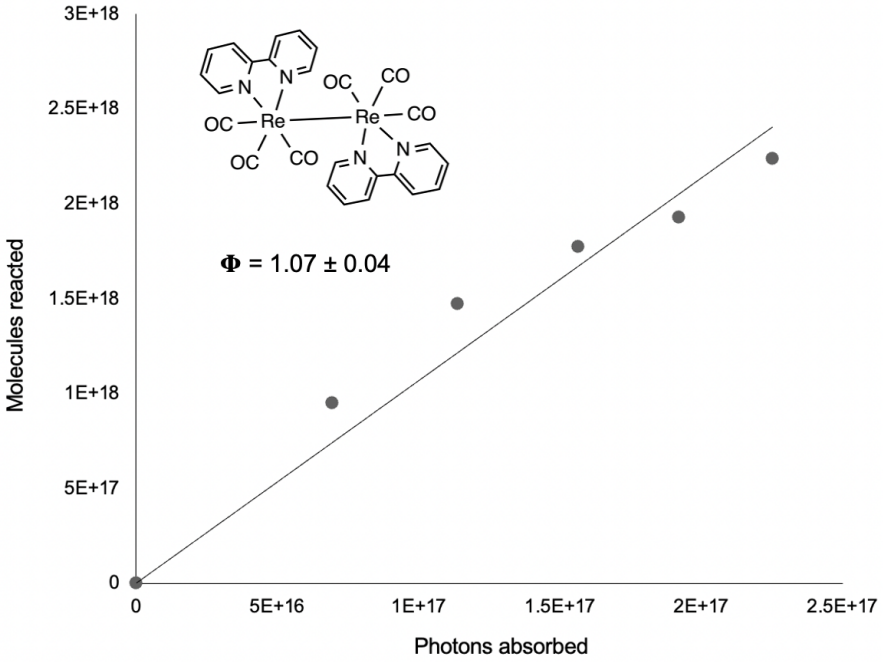

Figure 18. Quantum yield analysis of depletion of the MMLCT at 505 nm in an aerated solution of $[Re(CO)_3(bpy)]_2$. This line gives a slope of 1.07 ± 0.04, indicating that more photoreactions than incident photons took place.

Summary and Future Work

In this work, we synthesized a series of *fac*-$Re(CO)_3(L)Cl$ complexes (**1-7**) and Re-Mn dinuclear complexes that are candidates for photoCORMs: $(CO)_5MnRe(CO)_3(L)$ (compounds **6-8**). Similar to previously published dinuclear photoCORMs, visible light excitation of the $\sigma^{MM} \rightarrow \pi^{L^*}$ transition leads to homolytic

cleavage of the Re-Mn bond.[26] Although compounds $(CO)_5MnRe(CO)_3(L)$ does not show emission under irradiation, the photoproduct (**8**) displays an emission (λ_{max} = 555 nm). The dimeric complex $[Re(CO)_3bpy]_2$ (**9**) was also synthesized and investigated. As “turn-on” emissive photoCORMs, photochemical reaction and location of CO release and photoproducts can be monitored and tracked in biological targets. While other researchers have demonstrated similar turn-on emissions with photoCORMs, the present work extends the applicability to longer wavelengths in the therapeutic window.[18] In our work, broad and long wavelength ^{3}MLCT emission from rhenium photoproduct has high potential for imaging in biological study and emissive photoproducts of $(CO)_5MnRe(CO)_3(L)$ type complexes may also act as a photosensitizer to form singlet oxygen. In future, further characterization and study will be carried on the photoproduct of **6** to identify its structures and these photoCORMs will be studied in PLGA nano/micro carriers for biological application.

Increasing the polarity of the antenna ligands on such heterobimetallic complexes is of interest to investigate their effects on complex stability. In particular, the strongly electron-withdrawing nitro group should be assessed further as it has shown profound effects on the properties of other photochemical small molecule bioregulator (SMB) releasing compounds.[43] We are also interested in investigating the photophysical and CO releasing properties of $[(L)(CO)_3MnRe(CO)_3(L)]$ type complexes, in which an additional chromophoric ligand is attached to the Mn center.

III. H_2O_2-activated CORMs

A. Background

CO, as with other drug payloads, can be released through chemical activation. A particularly promising strategy for targeting disease states with overexpressed reactive oxygen species (ROS) is H_2O_2-activation of CORMs. Tumors are characterized by excessive metabolic activity. Since H_2O_2 is a byproduct of cell metabolism, it is seen to be overexpressed in cancer states. H_2O_2 also takes many roles in tumor growth.[36,58] The increased rate of H_2O_2 production and unique role in cancer growth means that tumors are also highly susceptible to changes in H_2O_2 concentration, thereby making selective targeting cancer states using H_2O_2-activated prodrugs a viable strategy for killing cancer cells.[37]

There have been few studies of H_2O_2's reactivity with metal carbonyls. Previous work in our group published by Barrett, et. al. explored the reaction mechanism of H_2O_2 with *fac*-[$Mn(CO)_3$(4,4'-$(COOH)_2$-2,2'-bipyridine)(Br)] (**10**) and proposed a few different possible rate-determining steps (RDSs) with strong pH dependence on which RDS was favored. Barrett, et. al. found that the second-order rate constant for the reaction of with *fac*-[$Mn(CO)_3$(4,4'-dicarboxyl-2,2'-bipyridine)(pyridine)]$^{2-}$ with H_2O_2 was an order of magnitude lower than the rate constant of the reaction of with **10** with H_2O_2. This observation suggests a correlation between the lability of ligands attached to the Mn center and their reactivity with H_2O_2. At pH 7.4, the products of the reaction between **10** and H_2O_2 were found to include Mn^{2+}, free 4,4'-$(COOH)_2$-bpy ligand, 2.5 equivalents CO, and an equivalent of CO_2. The presence of CO_2 among products indicates that at least some attack on the facial CO ligands occurs.

Substitution of the bromide ion in *fac*-[$Mn(CO)_3$(4,4'-dicarboxyl-2,2'-bipyridine)(Br)]$^{2-}$ by H_2O_2 and attack on a carbonyl by the peroxide are outlined as mechanisms for CO release from the manganese carbonyl.

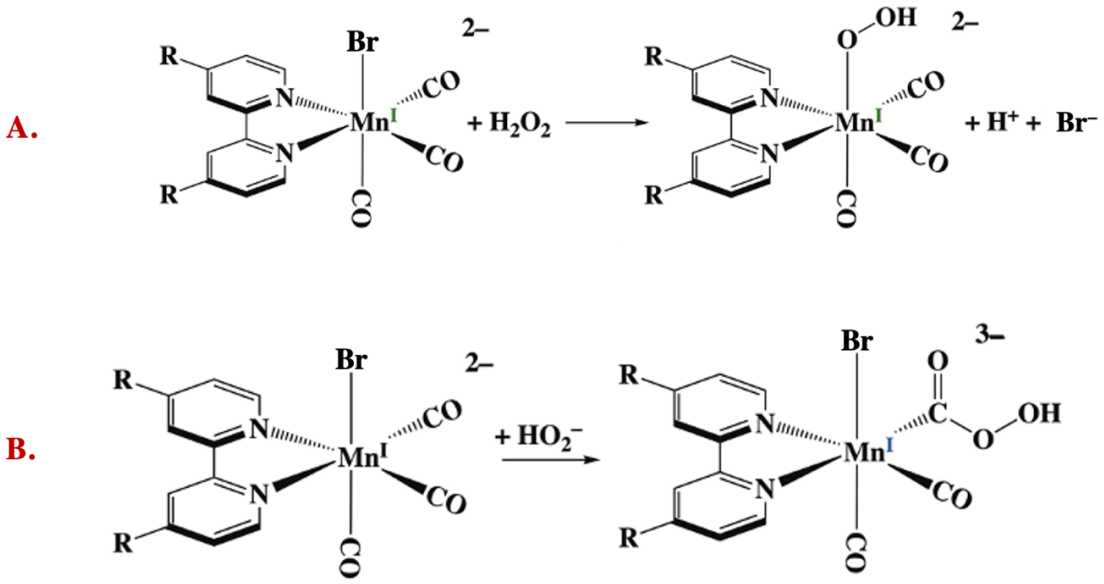

Figure 19. Two proposed RDSs by Barrett and coworkers regarding the reaction of **10** (R = COO^-) with H_2O_2: A. substitution of the bromide ligand with hydrogen peroxide and B. attack on a CO ligand by the hydroperoxy anion, HOO^-.

In this work, we present the manganese tetracarbonyl complex $Mn(CO)_4$(4,4'-$(COOH)_2$-bpy)][SbF_6] (**11**) and intend to use it to further characterize the reaction pathways taken by hydrogen peroxide with **10**. In the absence of the substitution pathway upon the reaction of $Mn(CO)_4$(4,4'-(COOH)2-bpy)] with H_2O_2, we expect to see a strong reduction in the reaction rate between this tetracarbonyl complex and H_2O_2. The change in reactivity between the tricarbonyl and tetracarbonyl complexes with H_2O_2 will yield insight into the reaction dynamics of H_2O_2 and this CO-releasing molecule.

B. Experimental

Materials

Manganese pentacarbonyl bromide was purchased from Strem Chemicals and used without further purification. 4,4'-dicarboxyl-2,2'-bipyridine was purchased from Ark Pharma, Inc. and used without further purification. Silver hexafluoroantimonate was purchased from Sigma-Aldrich Chemical Company and stored under an argon atmosphere. All solvents were purchased from Fisher Scientific. Dichloromethane (DCM) was dried by distillation over CaH_2 and stored over 3Å molecular sieves in an argon-atmosphere glove box. Methanol and toluene were stored over 3Å molecular sieves under ambient conditions.

Analytical Instrumentations

Solution optical absorption spectra were recorded in 1.0-cm-path-length quartz cells using a Shimadzu dual-beam UV-2401 PC. IR spectra were recorded using a JASCO FT/IR-4100; solution-phase spectra were collected using a KBr-windowed cell and mulls were created using mineral oil and KBr plates. Solution NMR spectra were also recorded on a 500 mHz Varian Unity Inova Spectrometer using a 5 mm Broadband Probe with pulsed field gradients.

Syntheses

$Mn(CO)_3(4,4'\text{-}(COOH)_2\text{-}bpy)(Br)$ (**10**) was synthesized according to previous procedures in this group.[45] A methanol solution of $Mn(CO)_5Br$ (0.4011 g, 1.459 mmol) was refluxed with a toluene solution of 4,4'-dicarboxyl-2,2'-bipyridine (0.3562 g, 1.459 mmol) for 2 hours under an argon atmosphere. The reaction mixture was cooled in a freezer overnight, then filtered. The filtrate was dried using a rotary

evaporator and washed with ether and hexanes to give a bright red powder, yielding 0.4041 g (59.8%).

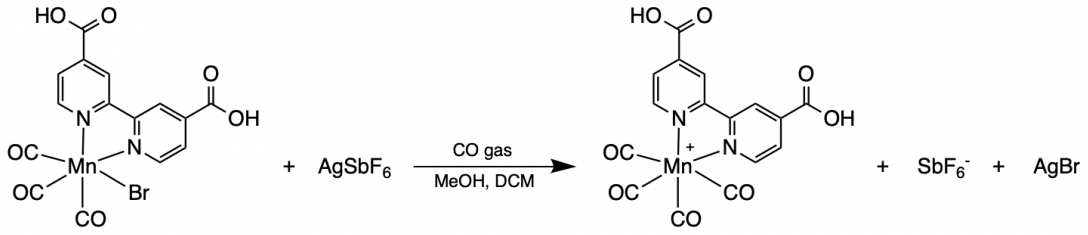

Figure 20. Synthetic scheme to form **11** upon reaction of **10** with $AgSbF_6$ and CO gas.

$[Mn(CO)_4(4,4'\text{-}(COOH)_2\text{-}bpy)][SbF_6]$ (**11**) was modified from a similar procedure deployed by Bocarsly and coworkers to synthesize $[Mn(CO)_4(bpy)][SbF_6]$.[59] A methanol solution of **10** (0.1359 g, 0.294 mmol) was added to a single-necked round-bottomed flask and saturated with CO. A DCM solution of $AgSbF_6$ (0.1576 g, 0.459 mmol) was added to the flask and stirred while bubbling with CO for 40 minutes in a tepid water bath. After 40 minutes, the bright red solution turned yellow and cloudy. The solution was filtered through a ground glass filter and concentrated under house vacuum, then extracted into 1:10 DCM/diethyl ether. The solution was stored overnight and a brick-red powdered was filtered off. The yellow supernatant was washed with water in triplicate and the aqueous phases were concentrated and layered with ether. A yellow powder was collected, yielding 34.5 mg (18%).

C. Results and Discussion

The synthesis afforded a yellow powder. In methanol, the UV-Visible spectrum of **11** shows a longest-wavelength band centered around 435 nm, slightly longer than the MLCT of **10** which is centered around 408 nm. The IR spectrum of

11 is also changed from the starting material. Fewer peaks in the carbonyl region are visible due to higher symmetry of **11** compared to **10**.

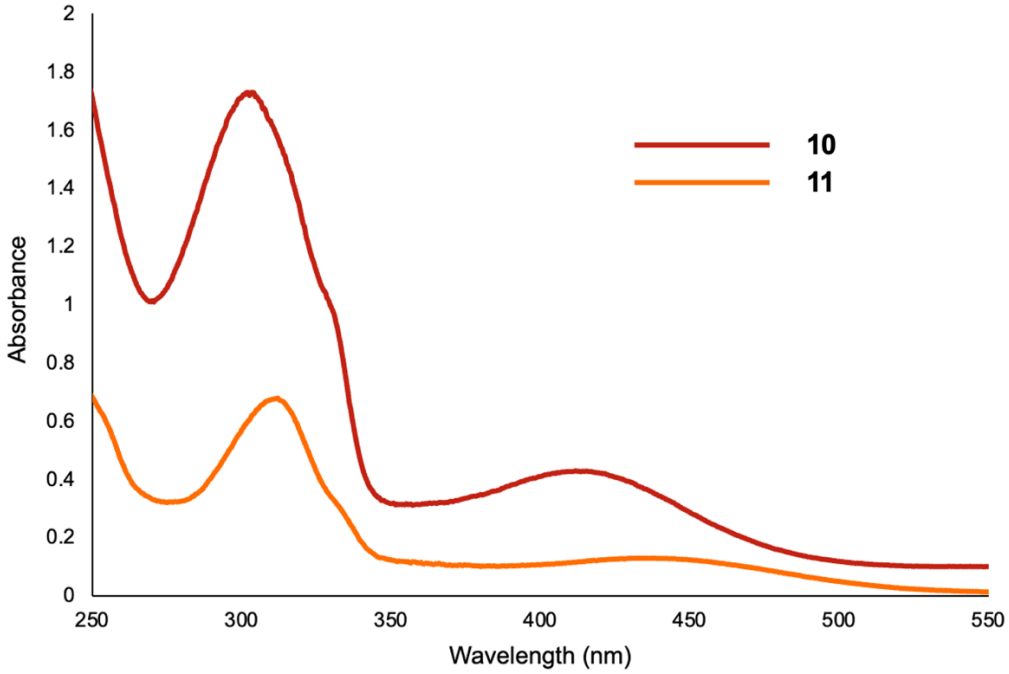

Figure 20. UV-Visible spectra of **10** and **11** in methanol. They show an MLCT transition at 408 nm and 435 nm, respectively.

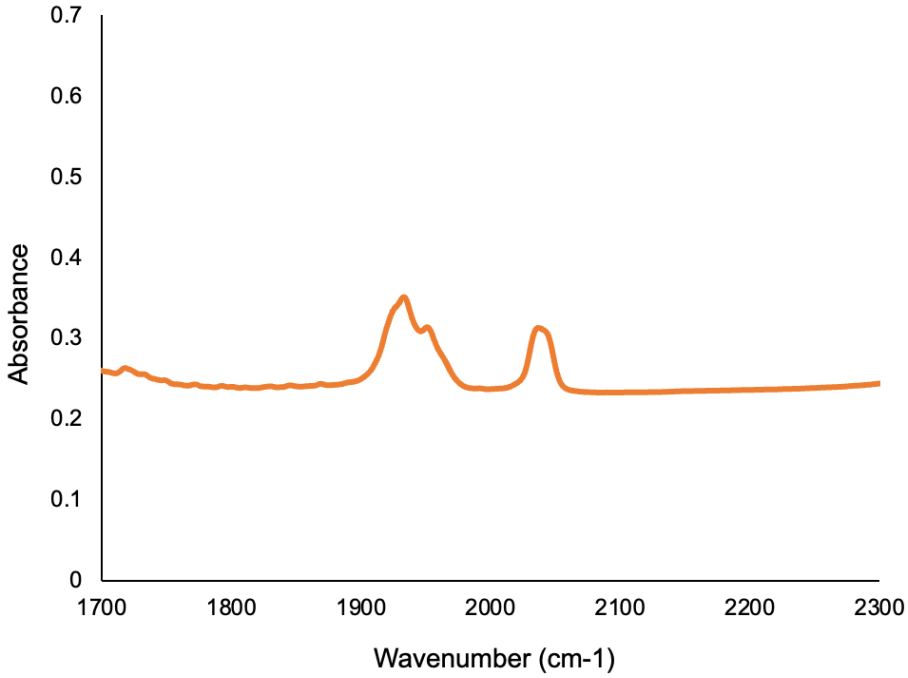

Figure 21. IR spectrum of **11** in a mineral oil mull. ν_{CO} = 1936, 1955, 2044 cm^{-1}.

To explore the mechanism of reaction of **11** with H_2O_2, similar experiments to those conducted by Barrett, et. al. must be undertaken, such as measuring the rate of disappearance of the MLCT at 435 nm of **11** upon reaction with H_2O_2 under varying pH conditions.[45] If the RDS of the reaction of **10** with H_2O_2 is indeed a substitution reaction under physiological conditions, we would expect to see a dramatically lower k_{obs} for the reaction of **11** with H_2O_2 under otherwise identical conditions.

D. Conclusion

Herein, we present a platform for investigating the H_2O_2 mediated redox reactions of **10** as well as studies into the photochemical behavior of group 7 metal-metal bonded complexes in aqueous solution. Further studies must be done to fully

utilize this diverse group of CORMs with multiple modes of activation. For example, pushing the wavelength of photoactivated CO-releasing molecules into the red is paramount to their viability as therapeutic agents. Additionally, in vitro and in vivo experiments must be done to explore biocompatibility and inertia towards non-deliberate physiological effects. The photoactivity of CORMs like **10** should also be explored to develop multifunctional therapies and exploit the precise control afforded by light-activation in addition to selective reactivity with H_2O_2.

IV. References

1. Olson, K. R. Carbon monoxide poisoning: Mechanisms, presentation, and controversies in management. *J. Emerg. Med.* **1984**, *1*(3), 233-243. DOI: https://doi.org/10.1016/0736-4679(84)90078-7

2. Ling, K.; Men, F.; Wang, W-C.; Zhou, Y-Q.; Zhang, H-W.; Ye, D-W. Carbon Monoxide and Its Controlled Release: Therapeutic Application, Detection, and Development of Carbon Monoxide Releasing Molecules (CORMs). *J. Med. Chem.* **2018**, *61*, 2611-2635. DOI: http://doi.org/10.1021/acs.jmedchem.6b01153

3. Snyder, S. H. Nitric Oxide: First in a New Class of Neurotransmitters? *Science.* **1992**, *257*, 494.

4. Ford, P. C. Metal complex strategies for photo-uncaging the small molecule bioregulators nitric oxide and carbon monoxide. *Coord. Chem. Rev.* **2018**, *376*, 548-564. DOI: https://doi.org/10.1016/j.ccr.2018.07.018

5. DeMartino, A. W.; Zigler, D. F.; Fukuto, J. M.; Ford, P. C. Carbon disulfide. Just toxic or also bioregulatory and/or therapeutic? *Chem. Soc. Rev.* **2017**, *46*(1), 21-39. DOI: https://doi.org/10.1039/C6CS00585C

6. Fukuto, J. M.; Carrington, S. J.; Tantillo, D. J.; Harrison, J. G.; Ignarro, L. J.; Freeman, B. A.; Chen, A.; Wink, D. A. Small Molecule Signaling Agents: The Integrated Chemistry and Biochemistry of Nitrogen Oxides, Oxides of Carbon, Dioxygen, Hydrogen Sulfide, and their Derived Species. *Chem. Res. Toxicol.* **2012**, *25*(4), 769-793. DOI: https://doi.org/10.1021/tx2005234

7. Motterlini, R.; Otterbein, L. E. The therapeutic potential of carbon monoxide. *Nat. Rev. Drug Discov.* **2010**, *9*, 728-743. DOI: https://doi.org/10.1038/nrd3228

8. Ford, P. C.; Pereira, C. M.; Miranda, K. M. Mechanisms of Nitric Oxide Reactions Mediated by Biologically Relevant Metal Centers. *Struct. Bond.* **2013**, *154*, 99-135. DOI: https://doi.org/10.1007/430_2013_117

9. Heinemann, S. H.; Hoshi, T.; Westerhausen, M.; Schiller, A. Carbon monoxide - physiology, detection, and controlled release. *Chem. Commun.* **2014**, *28*(50), 3644-3660. DOI: https://doi.org/10.1039/c3cc49196j

10. Otterbein, L.; Bach, F.; Alam, J.; Soares, M.; Lu, H. T.; Wysk, M.; Davis, R. J.; Flavell, R. A.; Choi, M. K. Carbon monoxide has anti-inflammatory effects involving the mitogen-activated protein kinase pathway. *Nat. Med.* **2000**, *6*, 422-428. DOI: https://doi.org/10.1038/74680

11. Vitek, L.; Gbelcova, H.; Muchova, L.; Vanova, K.; Zelenka, J.; Konickova, R.; Suk, J.; Zadinova, M.; Knejzlik, Z.; Ahmad, S.; Fujisawa, T.; Ahmed, A.; Ruml, T.

Antiproliferative effects of carbon monoxide on pancreatic cancer. *Dig. Liv. Disease.* **2014**, *46*(4), 369-375. DOI: https://doi.org/10.1016/j.dld.2013.12.007

12. Pinto, M. N.; Mascharak, P. K. Light-assisted and remote delivery of carbon monoxide to malignant cells and tissues: Photochemotherapy in the spotlight. J. *Photochem. Photobiol.* **2020**, *42*, 100341. DOI: https://doi.org/10.1016/j.jphotochemrev.2020.100341

13. Ford, P. C.; Garcia, J. V.; Guzman, C.; Kulkarni, S.; Wein, E. Photoactivated metal complexes for drug delivery. *Compr. Inorg. Chem. III.* **2022**, 1-43. DOI: https://doi.org/10.1016/B978-0-12-823144-9.00101-1

14. Pierri, A. E.; Muizzi, D. A.; Ostrowski, A. D.; Ford, P. C. Photo-Controlled Release of NO and CO with Inorganic and Organometallic Complexes. *Struct. Bond.* **2014**, *165*, 1-45. DOI: https://doi.org/10.1007/430_2014_164

15. Pierri, A. E.; Pallaoro, A.; Wu, G.; Ford, P. C. A Luminescent and Biocompatible PhotoCORM. *J. Am. Chem. Soc.* **2012,** *134*(44), 18197-18200. DOI: https://doi.org/19.1021/ja3084434

16. Zhu, X-H.; Du, J-X.; Zhu, D.; Ren, S-Z.; Chen, K.; Zhu, H-L. Recent Research on Methods to Improve Tumor Hypoxia Environment. *Oxid. Med. Cell. Longev.* **2020**, *2020*, 1-18. DOI: https://doi.org/10.1155/2020/5721258

17. Chiswell, B.; Huang, S-H. D. Manganese removal. *Interface Sci. Technol.* **2006**, *10*, 179-192. ISBN: 978-0-12-088380-6

18. Chakraborty, I.; Jimenez, J.; Sameera, W. M. C.; Kato, M.; Mascharak, P. K. Luminescent Re(I) Carbonyl Complexes as Trackable PhotoCORMs for CO delivery to Cellular Targets. *Inorg. Chem.* **2017**, *56*(5), 2863-2873. DOI: https://doi.org/10.1021/acs.inorgchem.6b02999

19. Carrington, S.; Chakraborty, I.; Bernard, J. M. L.; Mascharak, P. K. A Theranostic Two-Tone Luminescent PhotoCORM Derived from Re(I) and 92-Pyridyl)-benaothiazole: Trackable CO Delivery to Malignant Cells. *Inorg. Chem.* **2016**, *55*(16), 7852-7858. DOI: https://doi.org/10.1021/acs.inorgchem.6b00511

20. Rimmer, R. D.; Richter, H.; Ford, P. C. A Photochemical Precursor for Carbon Monoxide Release in Aerated Aqueous Media. *Inorg. Chem.* **2010**, *49*(3), 1180−1185. DOI: https://doi.org/10.1021/ic902147n

21. Zalis, S.; Farrell, I. R.; Vlcek, Jr. A. The Involvement of Metal-to-CO Charge Transfer and Ligand-Field Excited States in the Spectroscopy and Photochemistry of Mixed-Ligand Metal Carbonyls. A Theoretical and Spectroscopic Study of $[W(CO)_4$(1,2-ethylenediamine)] and $[W(CO)_4$(N,N'-bis-alkyl-1,4-diazabutadiene)]. *J. Am. Chem. Soc.* **2003**, *125*, 4580-4592. https://doi.org/10.1021/ja021022j

22. Gonzalez, M. A.; Yim, M. A.; Cheng, S.; Moyes, A.; Hobbs, A. J.; Mascharak, P. K. Manganese Carbonyls Bearing Tripodal Polypyridine Ligands as Photoactive Carbon Monoxide-Releasing Molecules. *Inorg. Chem.* **2011**, *51*, 601-608. DOI: https://doi.org/10.1021/ic2021287

23. D'Orazio, J.; Jarrett, S.; Amaro-Ortiz, A.; Scott, T. UV Radiation and the Skin. *Int. J. Mol. Sci.*, **2013**, *14*(6), 12222-12248. DOI: https://doi.org/10.3390/ijms140612222

24. Konig, K. J. Multiphoton microscopy in life sciences. *J. Microsc.* **2000**, *200*(2), 83-104. DOI: https://doi.org/10.1046/j.1365-2818.2000.00738.x

25. Jiang, Q.; Xia, Y.; Barrett, J.; Mikhailovsky, A.; Wu, G.; Wang, D.; Shi, P.; Ford, P. C. Near-Infrared and Visible Photoactivation to Uncage Carbon Monoxide from an Aqueous-Soluble PhotoCORM. *Inorg. Chem.* **2019**, *58*, 11066-11075. DOI: https://doi.org/10.1021/acs.inorgchem.9b01581

26. Li, Z.; Pierri, A. E.; Huang, P-J.; Wu, G.; Iretskii, A. V.; Ford, P. C. Dinuclear PhotoCORMs: Dioxygen-Assisted Carbon Monoxide Uncaging from Long-Wavelength-Absorbing Metal-Metal-Bonded Carbonyl Complexes. *Inorg. Chem.* **2017**, *56*(11), 6094-6104. DOI: https://doi.org/10.1021/acs.inorgchem.6b03138

27. Marker, S. C.; MacMillan, S. N.; Zipfel, W. R.; Li, Z.; Ford, P. C.; Wilson, J. J. Photoactivated in Vitro Anticancer Activity of Rhenium(I) Tricarbonyl Complexes Bearing Water-Soluble Phosphines. *Inorg. Chem.* **2018**, *57*(3), 1311-1331. DOI: https://doi.org/10.1021/acs.inorgchem.7b02747

28. Lee, L. C. Leung, K-K.; Lo, K. Recent development of luminescent rhenium(i) tricarbonyl polypyridine complexes as cellular imaging reagents, anticancer drugs, and antibacterial agents. *Dalton Trans.* **2017**, *46*, 16357-16380. DOI: https://doi.org/10.1039/C7DT03465B

29. Li, Z. Towards Long Wavelength Absorption: Dinuclear Photo-activated CO Releasing Moieties. Ph.D Dissertation, UC Santa Barbara, Santa Barbara, CA, 2018.

30. Garcia, J. V.; Yang, J.; Shen, D; Chi, Y.; Li, X.; Wang, R.; Stucky, G. D.; ZHao, D.; Ford, P. C.; Zhang, F. NIR-Triggered Release of Caged Nitric Oxide using Upconverting Nanostructured Materials. *Small*. **2012**, *8*(24), 3800-3805. DOI: https://doi.org/10.1002/smll.201201213

31. Coffey, K. E.; Moreira, R.; Abbas, F. Z.; Murphy, G. K. Synthesis of 3,3-dichloroindolin-2-ones from isatin-3-hydrazones and (dichloroiodo)benzene. *Org. Biomol. Chem.* **2015**, *13*(3), 682-685. DOI: https://doi.org/10.1039/C4OB02213K

32. Garcia, J. V.; Zhang, F.; Ford, P. C. Multi-photon excitation in uncaging the small molecule bioregulator nitric oxide. *Philos. Trans. Royal Soc. A.* **2013**, *371*, 1-25. http://dx.doi.org/10.1098/rsta.2012.0129

33. Xu, C.; Webb, W. W. Measurement of two-photon excitation cross sections of molecular fluorophores with data from 690 to 1050 nm. *J. Opt. Soc. Am. B.* **1996**, *13*(3), 481-491. DOI: https://doi.org/10.1364/JOSAB.13.000481

34. Wu, L.; Liu, J.; Li, P.; Tang, B.; James, T. D. Two-photon small-molecule fluorescence-based agents for sensing, imaging, and therapy within biological systems. *Chem. Soc. Rev.* **2021**, *50*, 702-734. DOI: https://doi.org/10.1039/D0CS00861C

35. Gonzalez, M. A.; Fry, N. L.; Burt, R.; Davda, R.; Hobbs, A.; Mascharak, P. K. Designed Iron Carbonyls as Carbon Monoxide (CO) Releasing Molecules: Rapid CO Release and Delivery to Myoglobin in Aqueous Buffer, and Vasorelaxation of Mouse Aorta. *Inorg. Chem.* **2011**, *50*(7), 3127-3134. https://doi.org10.1021/ic2000848

36. Szatrowski, T. P.; Nathan, C. F. Production of large amounts of hydrogen peroxide by human tumor cells. *Cancer Res.* **1991**, *51*(3), 794-798.

37. Rahn, J.; Lichtenfels, R.; Wessjohann, L. A.; Seliger, B. Hydrogen peroxide - production, fate and role in redox signaling of tumor cells. *Cell Commun. Signal.* **2015**, *13*(39), 1-19. DOI: https://doi.org/10.1186/s12964-015-0118-6

38. Altmann, E.; Aichholz, R.; Betschart, C.; Buhl, T.; Green, J.; Lattmann, R.; Missbach, M. Dipeptide nitrile inhibitors of cathepsin K. *Bioorg. Med. Chem. Lett.* **2006**, *16*, 2549–2554. DOI: https://doi.org/10.1016/j.bmcl.2006.01.104

39. Respondek, T.; Garner, R. N.; Herroon, M. K.; Podgorski, I.; Turro, C.; Kodanko, J. J. Light Activation of a Cysteine Protease Inhibitor: Caging of a Peptidomimetic Nitrile with $Ru^{II}(bpy)_2$. *J. Am. Chem. Soc.* **2011**, *133*, 17164–17167. DOI: https://doi.org/10.1021/ja208084s

40. Respondek, T.; Sharma, R.; Herroon, M. K.; Garner, R. N.; Knoll, J. D.; Cueny, E.; Turro, C.; Podgorski, I.; Kodanko, J. J. Inhibition of Cathepsin Activity in a Cell-Based Assay by a Light-Activated Ruthenium Compound. *ChemMedChem* **2014**, *9*, 1306–1315. DOI: https://doi.org/10.1002%2Fcmdc.201400081

41. Sharma, R.; Knoll, J. D.; Martin, P. D.; Podgorski, I.; Turro, C.; Kodanko, J. J. Ruthenium Tris(2-pyridylmethyl)amine as an Effective Photocaging Group for Nitriles. *Inorg. Chem.* **2014**, *53*, 3272–3274. DOI: https://doi.org/10.1021%2Fic500299s

42. Olesen, U. H.; Christensen, M. K.; Björkling, F.; Jäättelä, M.; Jensen, P. B.; Sehested, M.; Nielsen, S. J. Anticancer agent CHS-828 inhibits cellular synthesis of

NAD. *Biochem. Biophys. Res. Commun.* **2008**, *367*(4), 799-804. DOI: https://doi.org/10.1016/j.bbrc.2008.01.019

43. Jin, Z.; Wen, Y.; Xiong, L.; Yang, T.; Zhao, P.; Tan, L.; Wang, T.; Qian, Z.; Su, B-L.; He, Q. Intratumoral H_2O_2-triggered release of CO from a metal carbonyl-based nanomedicine for efficient CO therapy. *Chem. Commun.* **2017**, *40*(53), 5557–5560. DOI: https://doi.org/10.1039/C7CC01576C

44. Jin, Z.; Zhao, P.; Zhang, J.; Yang, T.; Zhou, G.; Zhang, D.; Wang, T.; He, Q. Intelligent metal carbonyl metal-organic framework nanocomplex for fluorescent traceable H2O2 triggered CO delivery. *Chem. Eur. J.* **2018,** *24*(45), 11667-11674. DOI: https://doi.org/10.1002/chem.201801407

45. Barrett, J. A.; Li, Z.; Garcia, J. V.; Wein, E.; Zheng, D.; Hunt, C.; Ngo, L.; Sepunaru, L.; Iretskii, A. V.; Ford, P. C. Redox-mediated carbon monoxide release from a manganese carbonyl–implications for physiological CO delivery by CO releasing moieties. *R. Soc. Open Sci.* **2021**, *8*, 1-14. DOI: https://doi.org/10.1098/rsos.211022

46. Wu D et al. Mesoporous polydopamine carrying manganese carbonyl responds to tumor microenvironment for multimodal imaging- guided cancer therapy. *Adv. Funct. Mater.* 2019, *29*, 1900095. DOI: https://doi.org/10.1002/adfm.201900095

47. Ma, G.; Liu, Z.; Zhu, C.; Chen, H.; Kwok, R. T. K.; Zhang, P.; Tang, B. Z.; Cai, L.; Gong, P. H_2O_2-Responsive NIR-II AIE Nanobomb for Carbon Monoxide Boosting Low-Temperature Photothermal Therapy. *Angew. Chem. Intl. Ed.* **2022**, *61*(36), e202207213. DOI: https://doi.org/10.1002/anie.202207213

48. Motterlini, R.; Clark, J. E.; Foresti, R.; Sarahchandra, P.; Mann, B. E.; Green, C. J. Carbon Monoxide-Releasing Molecules: Characterization of Biochemical and Vascular Activities. *Circ. Res.* **2002**, *90*(2), e17-e24. DOI: https://doi.org/10.1161/hh0202.104530

49. Wright, M. A.; Wright, J. A. PhotoCORMS: CO release moves into the visible. *Dalton. Trans.* **2016**, *45*(16), 6801-6811. DOI: https://doi.org/10.1039/C5DT04849D

50. Slanina, T.; Šebej, P. Visible-light-activated photoCORMs: rational design of CO-releasing organic molecules absorbing in the tissue-transparent window. *Photochem. Photobiol. Sci.* **2018**, *17*, 692-710. DOI: https://doi.org/10.1039/c8pp00096d

51. Peng, P.; Wang, C.; Shi, Z.; Johns, V. K.; Ma, L.; Oyer, J.; Copik, A.; Igarashi, R.; Liao, Y. Visible-light activatable organic CO-releasing molecules (photoCORMs) that simultaneously generate fluorophores. *Org. Biomol. Chem.* **2013**, *11*(39), 6671-6674. DOI: https://doi.org/10.1039/C3OB41385C

52. Lazarus, L. S.; Esquer, H. J.; Anderson, S. N.; Berreau, L. M.; Benninghoff, A. D. Mitochondrial-Localized Versus Cytosolic Intracellular CO-Releasing Organic PhotoCORMs: Evaluation of CO Effects Using Bioenergetics. *ACS Chem. Biol.* **2018**, *13*(8), 2220-2228. DOI: https://doi.org/10.1021/acschembio.8b00387

53. Anderson, S. N.; Richards, J. M.; Esquer, H. J.; Benninghoff, A. D.; Arif, A. M.; Berreau, L. M. A Structurally-Tunable 3-Hydroxyflavone Motif for Visible Light-Induced Carbon Monoxide-Releasing Molecules (CORMs). *ChemistryOpen.* **2015**, *4*(5), 590-594. DOI: https://doi.org/10.1002/open.201500167

54. Bauer, N.; Yang, X.; Yuan, Z.; Wang, B. Reassessing CORM-A1: redox chemistry and idiosyncratic CO-releasing characteristics of the widely used carbon monoxide donor. *Chem. Sci.* **2023**, *14*(12), 3215-3228. DOI: https://doi.org/10.1039/D3SC00411B

55. Kottelat, E.; Fabio, Z. Visible Light-Activated PhotoCORMs. *Inorganics*. **2017**, *5*(2), 24-43. DOI: https://doi.org/10.3390/inorganics5020024

56. Yi, X.; Zhao, J.; Sun, J.; Guo, S.; Zhang, H. Visible Light-Absorbing Rhenium Tricarbonyl Complexes as Triplet Photosensitizers in Photooxidation and Triplet-Triplet Annihilation Upconversion. *Dalton. Trans.* **2013**, *42*, 2062-2074. DOI: https://doi.org/10.1039/C2DT32420B

57. Smith, G. F.; Cagle Jr., F. Wm. The Improved Synthesis of 5-nitro-1,10-phenanthroline. J. Org. Chem. **1947**, *12*(6), 781-784. DOI: https://doi.org/10.1021/jo01170a007

58. Lennicke, C.; Rahn, J.; Lichtenfels, R.; Wessjohann, L. A.; Seliger, B. Hydrogen peroxide – production, fate and role in redox signaling of tumor cells. *Cell. Commun. Signal.* **2015**, *13*(39). DOI: https://doi.org/10.1186/s12964-015-0118-6

59. Kuo, H-Y.; Tignor, S. E.; Lee, T. S.; Ni, D.; Park, J. E.; Scholes, G. D.; Bocarsly, A. B. Reduction-induced CO dissociation by a $[Mn(bpy)(CO)_4][SbF_6]$ complex and its relevance in electrocatalytic CO_2 reduction. *Dalton. Trans.* **2020**, *49*, 891-900. DOI: https://doi.org/10.1039/c9dt04150h

V. Appendix

Contents

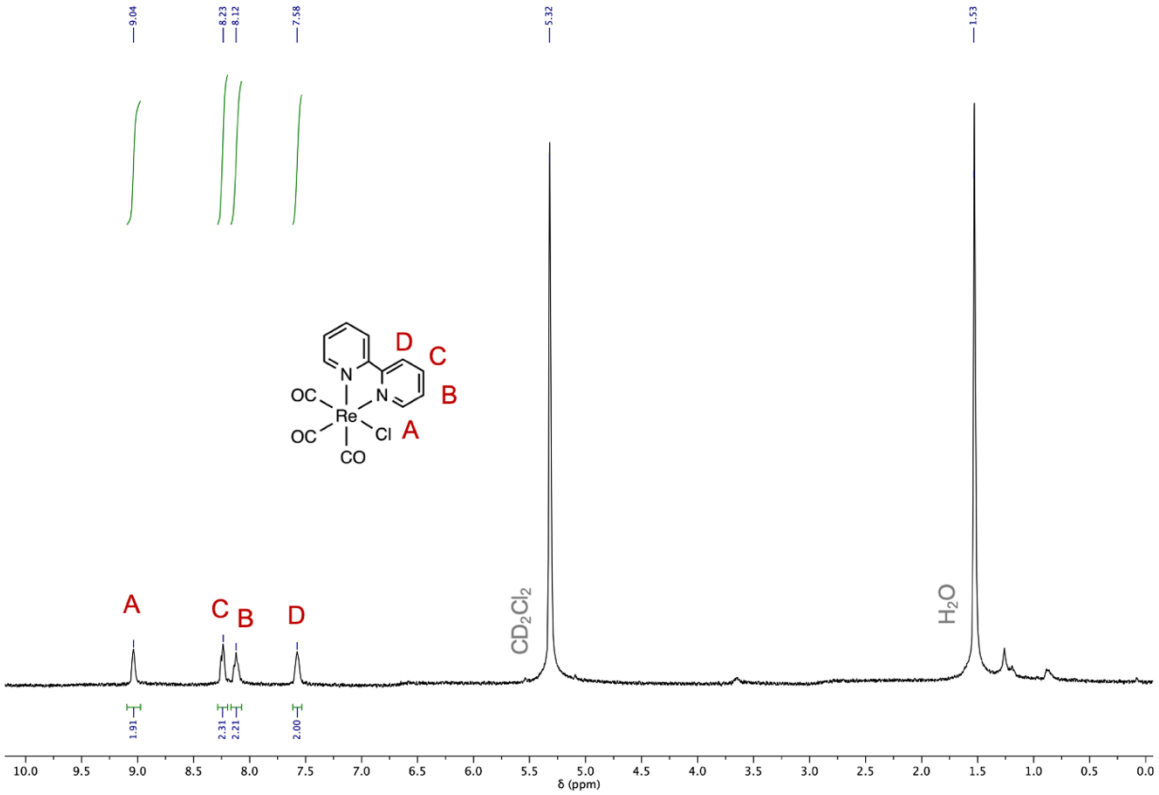

Figure A1. ^{1}H-NMR spectrum of *fac*-[Re(CO)$_3$(bpy)Cl] in CD_2Cl_2.

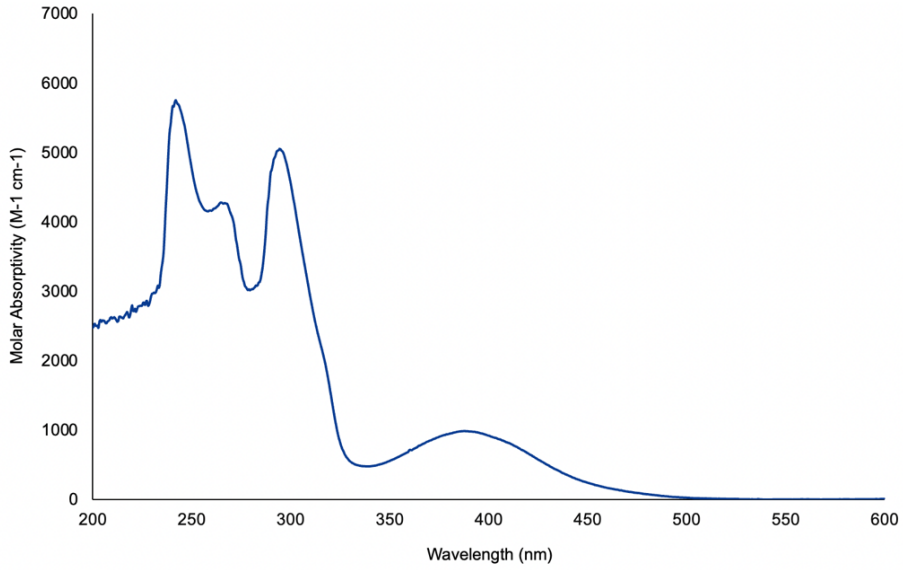

Figure A2. UV-Visible spectrum of *fac*-[Re(CO)$_3$(bpy)Cl] (4.04 x 10^{-4} M, THF). $\boldsymbol{\lambda}_{max}$(MLCT) = 388 nm (989 M^{-1} cm^{-1})

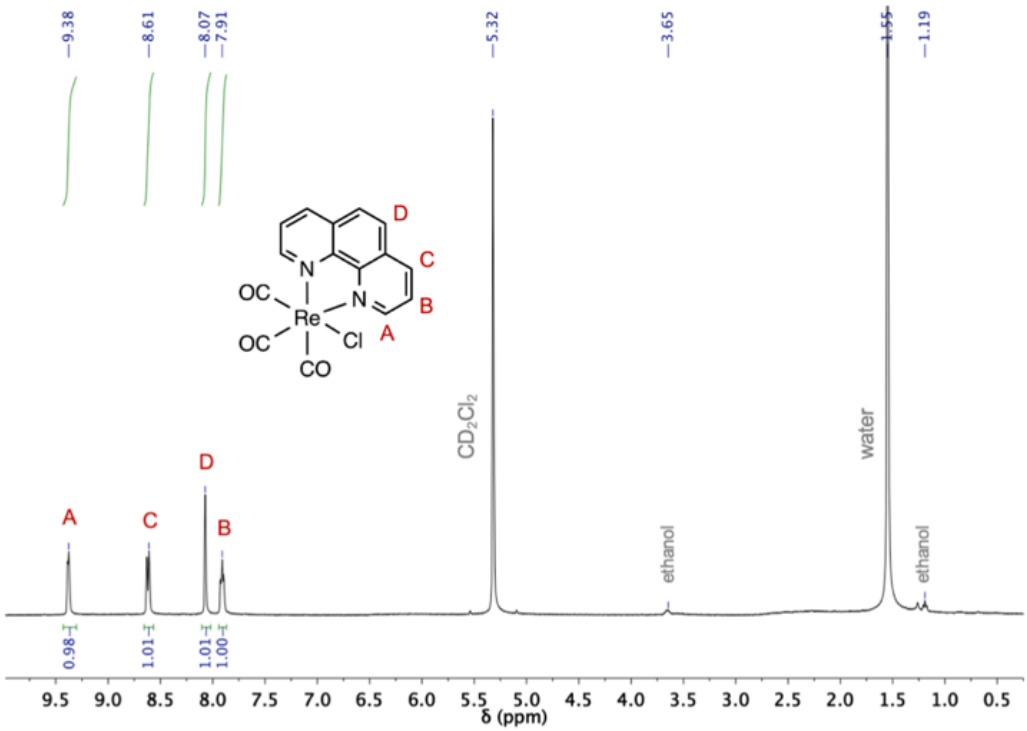

Figure A3. ^{1}H-NMR spectrum of *fac*-[Re(CO)$_3$(phen)Cl] in CD_2Cl_2.

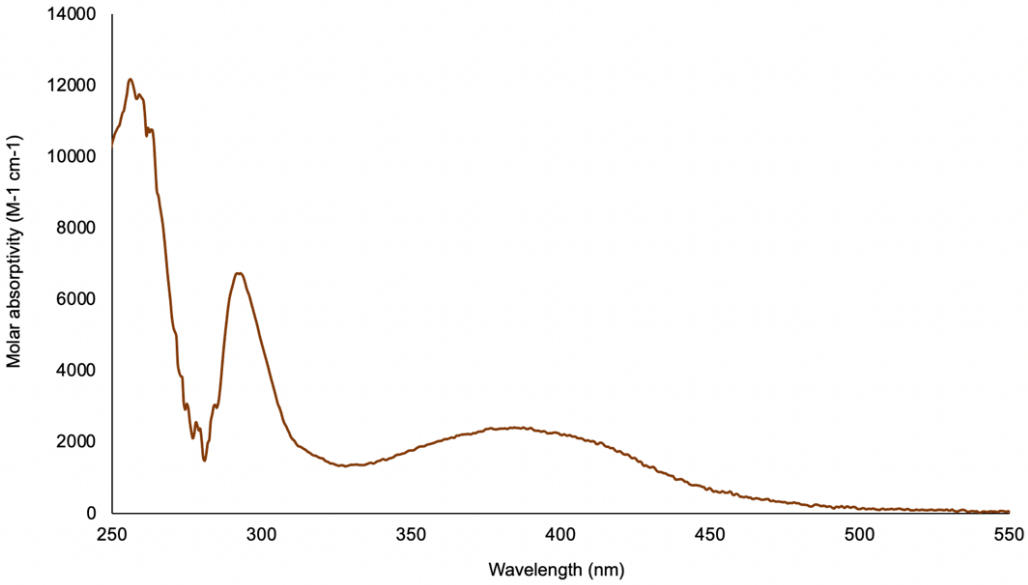

Figure A4. UV-Visible spectrum of *fac*-[Re(CO)$_3$(phen)Cl] (9.88 x 10^{-4} M, THF). $\boldsymbol{\lambda}_{max}$(MLCT) = 387.5 nm (2400 M^{-1} cm^{-1})

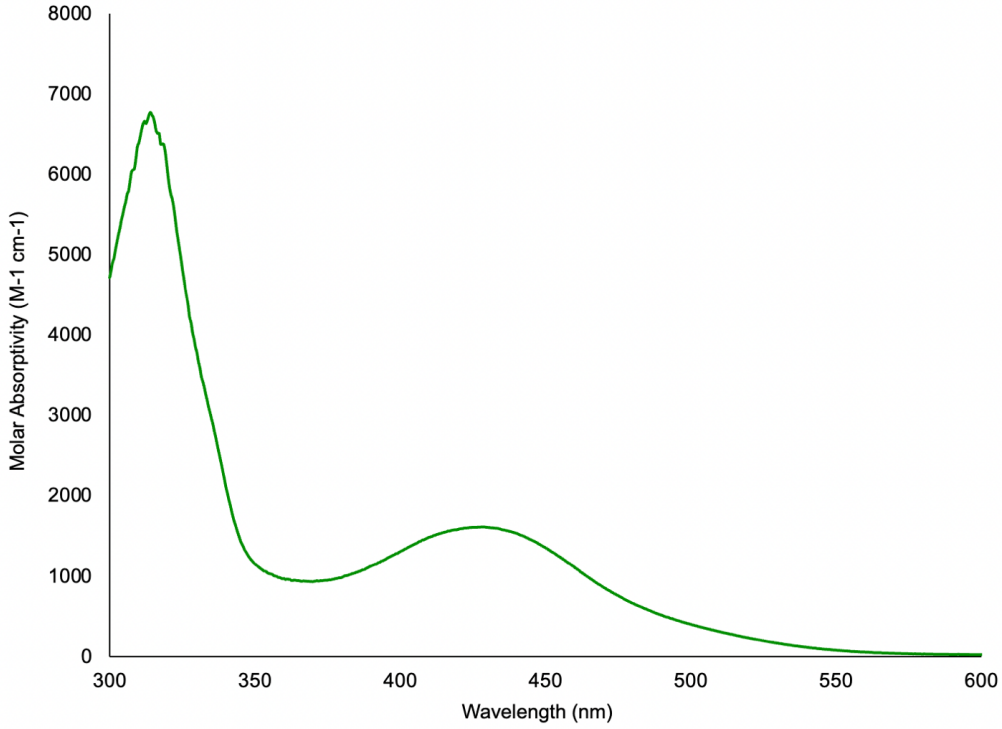

Figure A5. UV-Visible spectrum of *fac*-[$Re(CO)_3$(5,5'-bpy-$(COOH)_2$)Cl] (4.50 x 10^{-4} M, THF). λ_{max}(MLCT) = 428 nm (1609 M^{-1} cm^{-1})

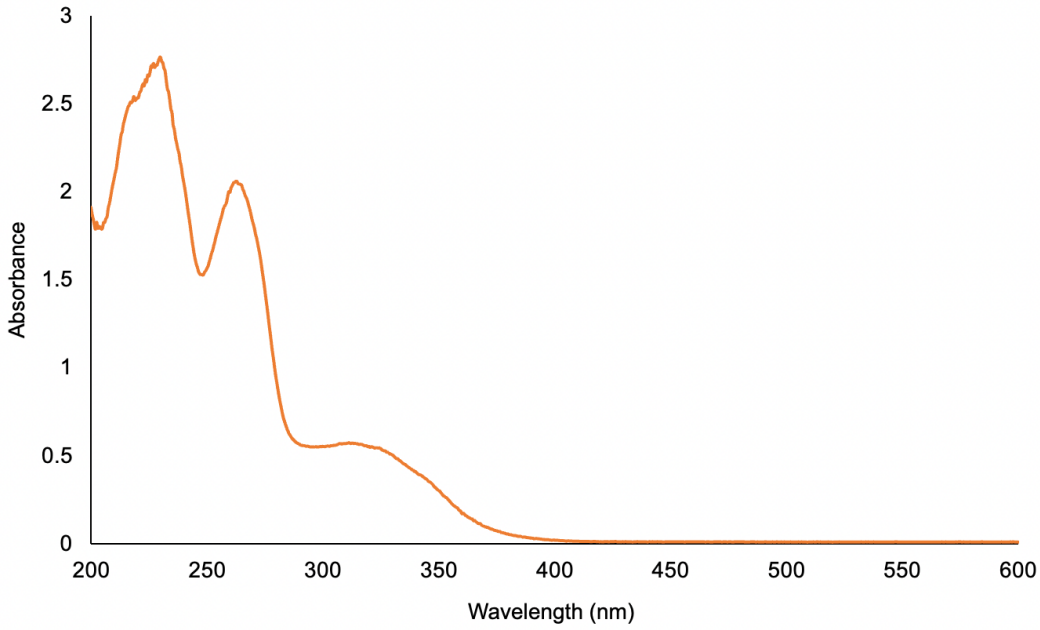

Figure A6. Qualitative UV-Visible spectrum of 5-nitro-phenanthroline (MeCN).

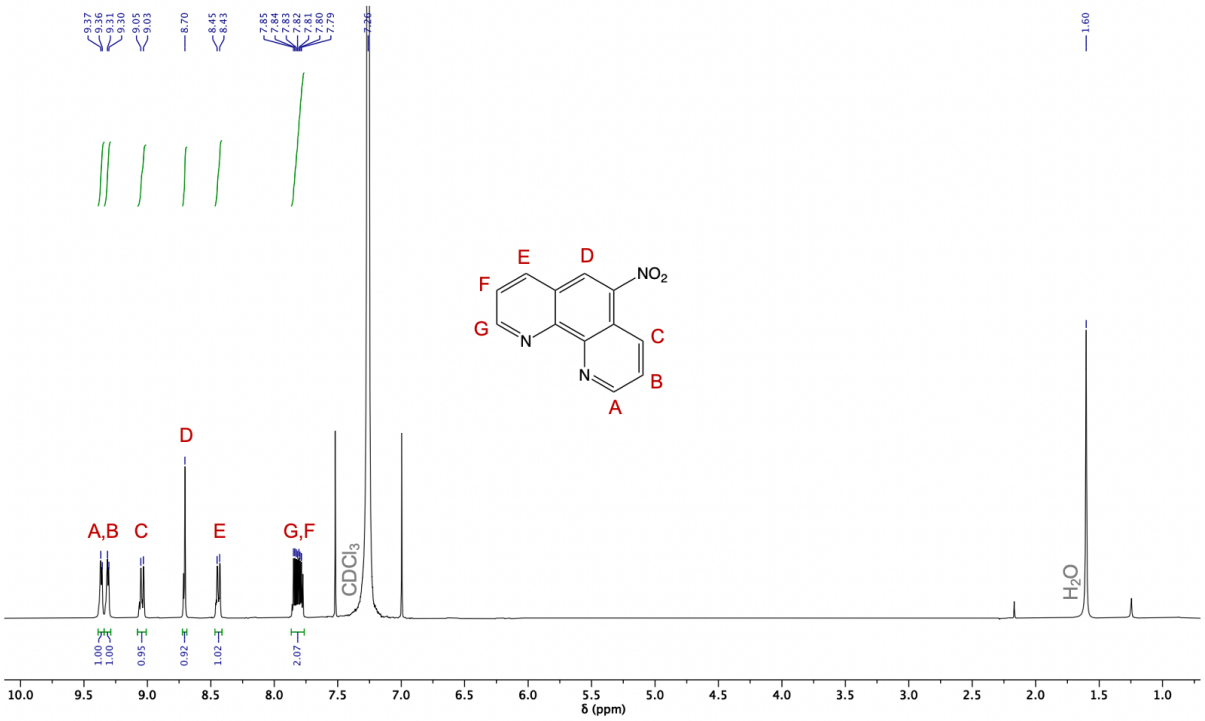

Figure A7. ^{1}H-NMR spectrum of 5-nitro-phenanthroline in $CDCl_3$.

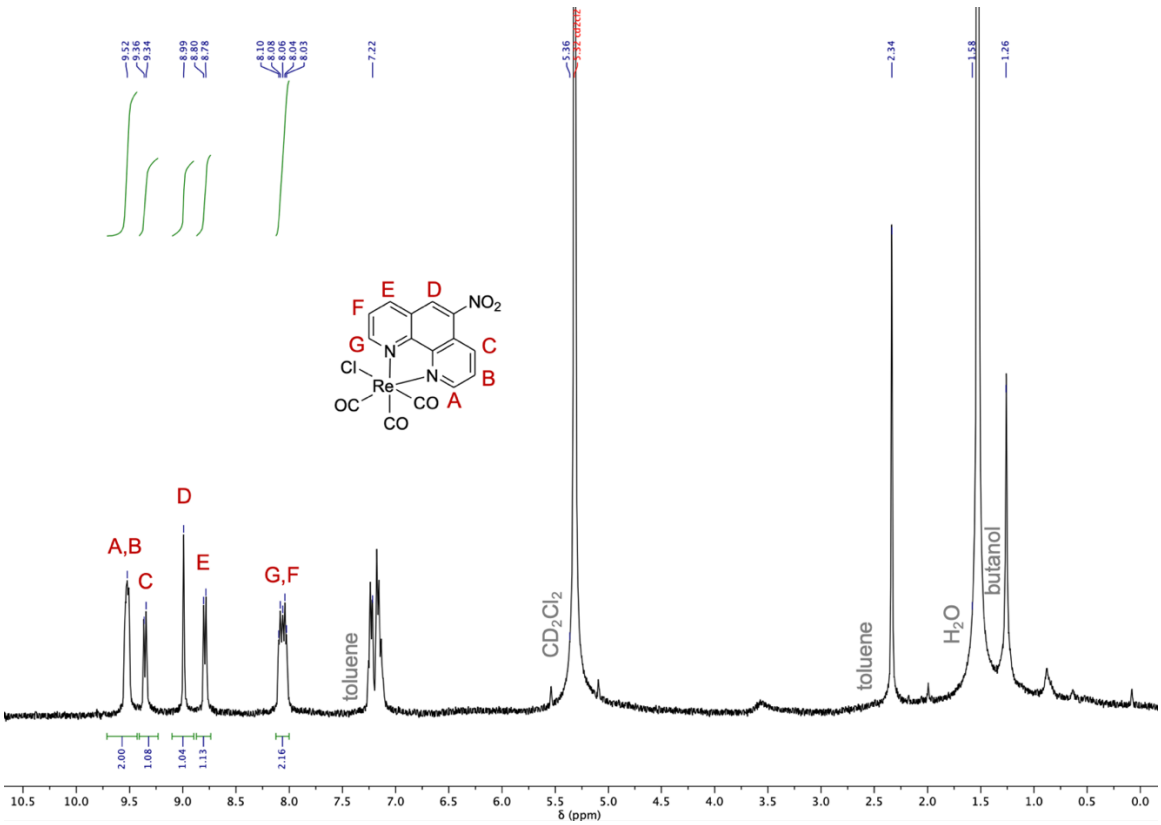

Figure A8. ^{1}H-NMR spectrum of *fac*-[$Re(CO)_3$(phen-NO_2)Cl] in CD_2Cl_2.

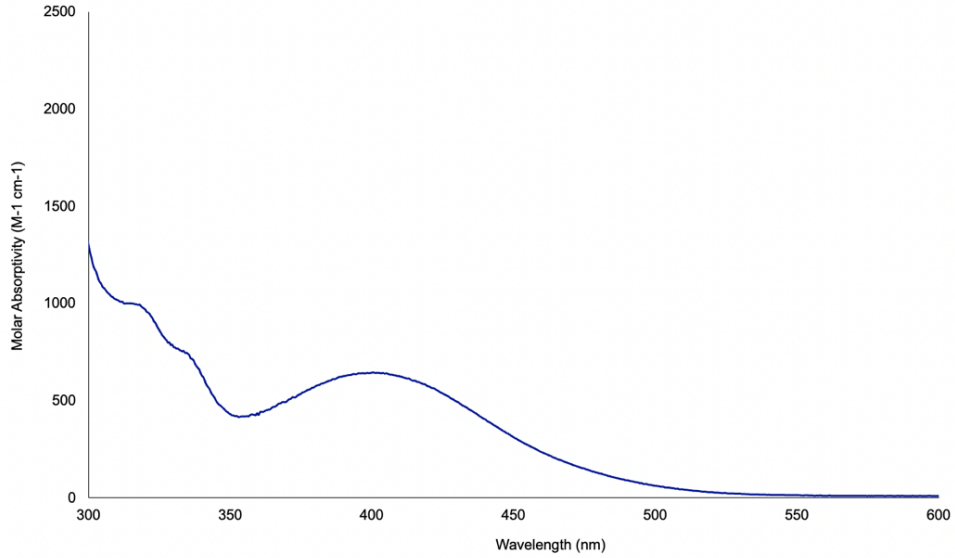

Figure A9. UV-Visible spectrum of *fac*-[$Re(CO)_3(phen\text{-}NO_2)Cl$] (7.50 x 10^{-4} M, THF). λ_{max}(MLCT) = 400.5 nm (644 M^{-1} cm^{-1})

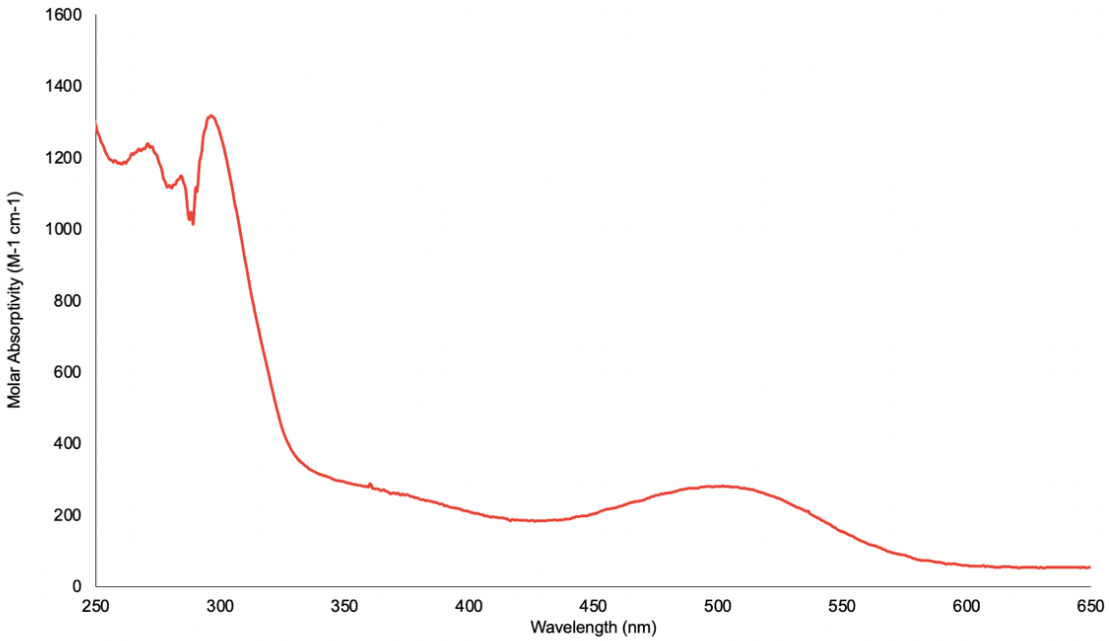

Figure A10. UV-Visible spectrum of putative $(CO)_5MnRe(CO)_3bpy$ (5.30 x 10^{-4} M, THF). λ_{max}(MMLCT) = 502 nm (281 M^{-1} cm^{-1})

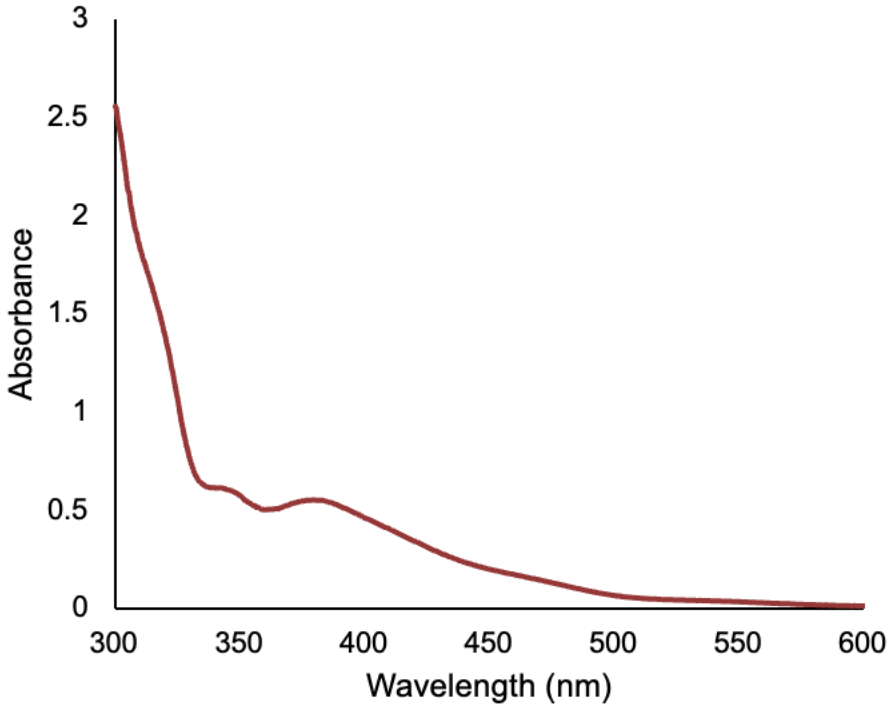

Figure A11. Qualitative UV-Visible spectrum of putative $(CO)_5MnRe(CO)_3(phen)$ (CH_3CN).

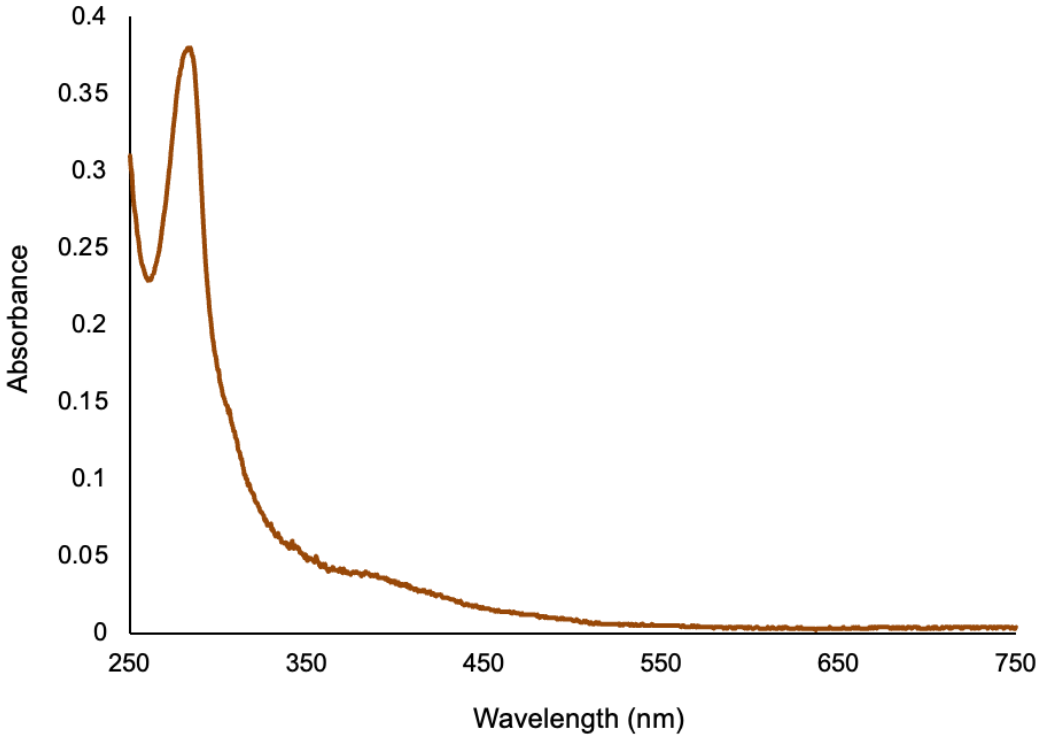

Figure A12. Qualitative UV-Visible spectrum of putative $(CO)_5MnRe(CO)_3(5\text{-}phen\text{-}Br)$ (CH_3CN).

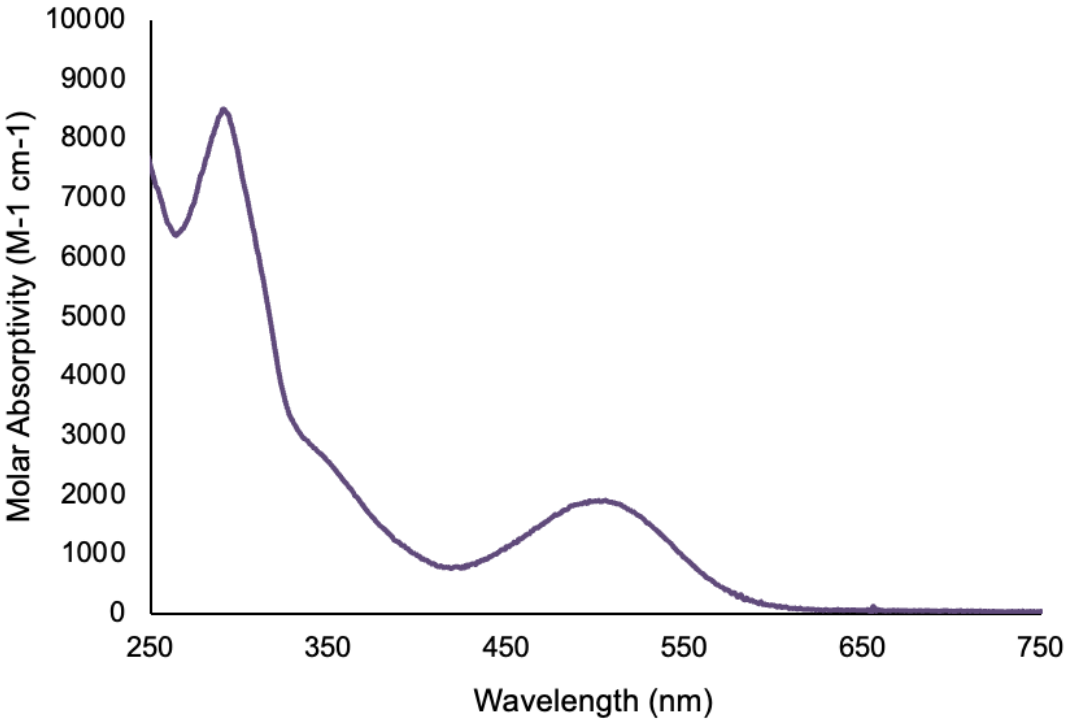

Figure A13. UV-Visible spectrum of $[Re(CO)_3bpy]_2$ (1.76 x 10^{-4} M, CH_3CN). λ_{max}(MMLCT) = 505 nm (1910 M^{-1} cm^{-1})

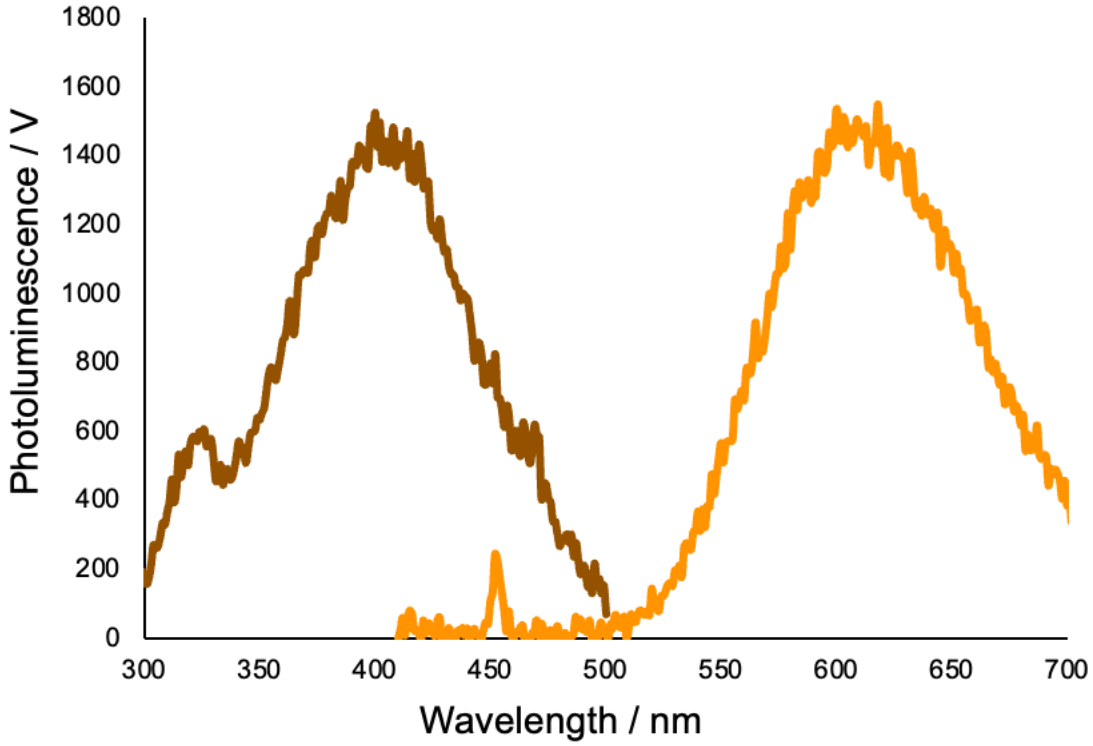

Figure A14. Photoluminescence of *fac*-[Re(CO)$_3$bpyCl] upon excitation at 400 nm (orange) and the excitation spectrum detected at 610 nm (brown).

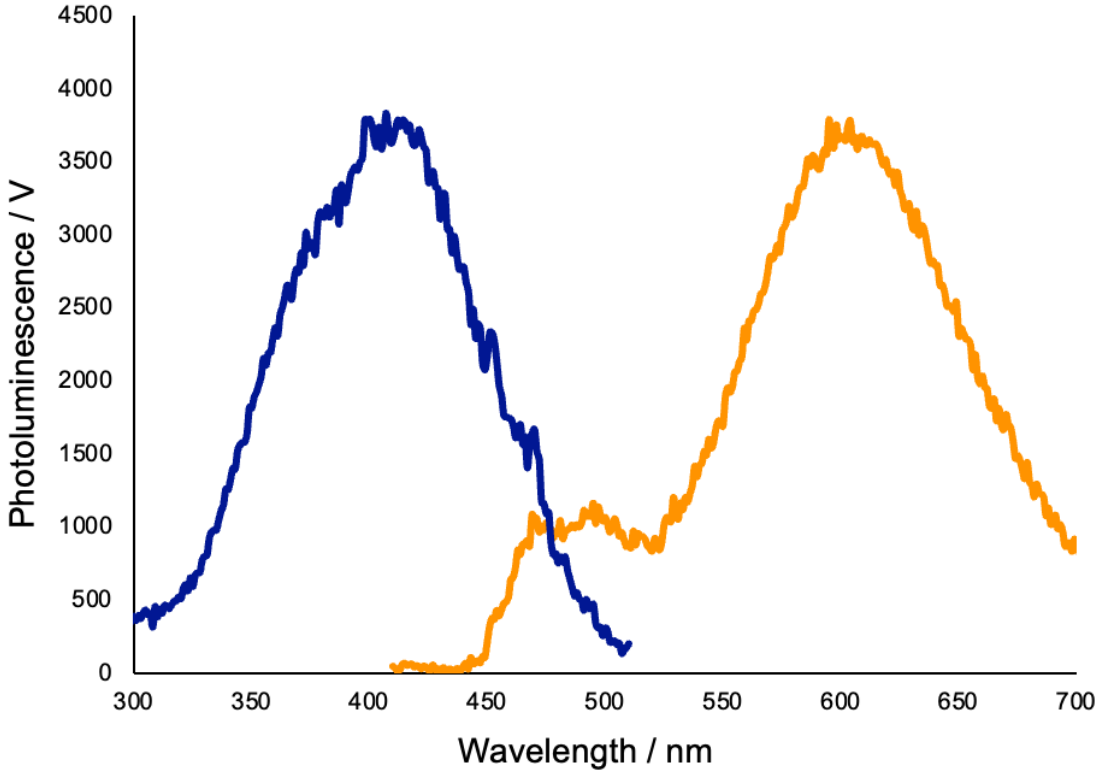

Figure A15. Photoluminescence of *fac*-[Re(CO)$_3$(phen)Cl] upon excitation at 400 nm (orange) and the excitation spectrum detected at 600 nm (blue).

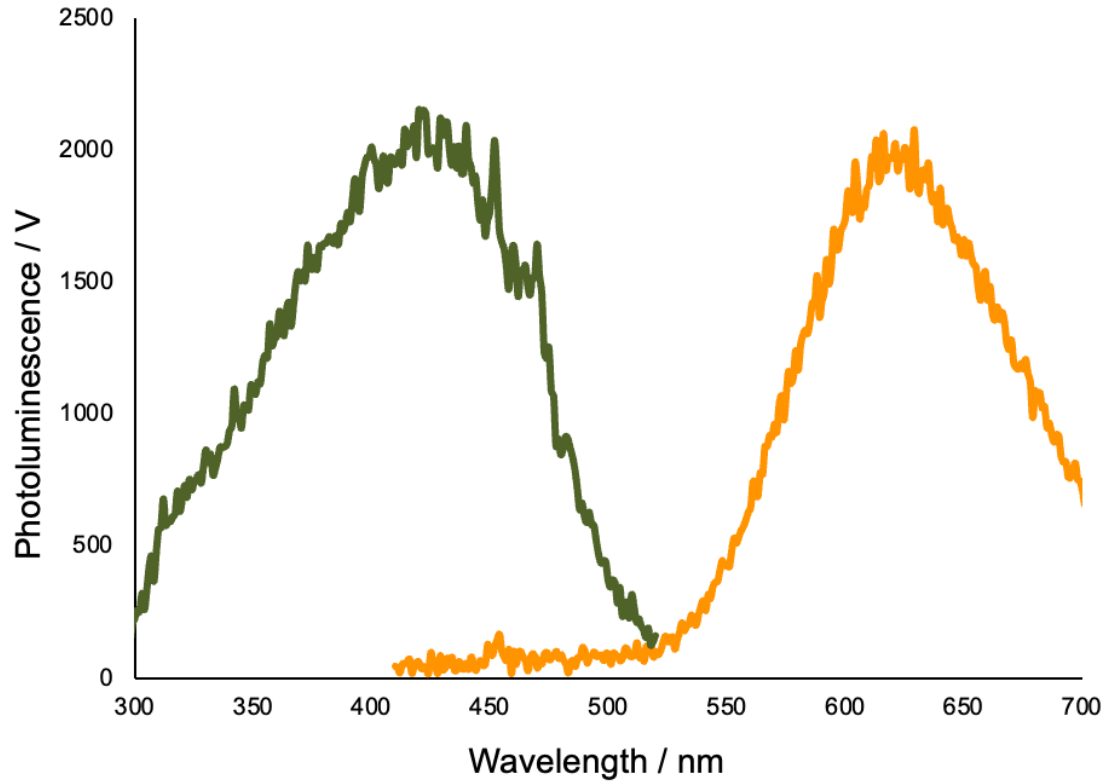

Figure A16. Photoluminescence of *fac*-[Re(CO)$_3$(5-phen-Br)Cl] upon excitation at 400 nm (orange) and the excitation spectrum detected at 620 nm (green).

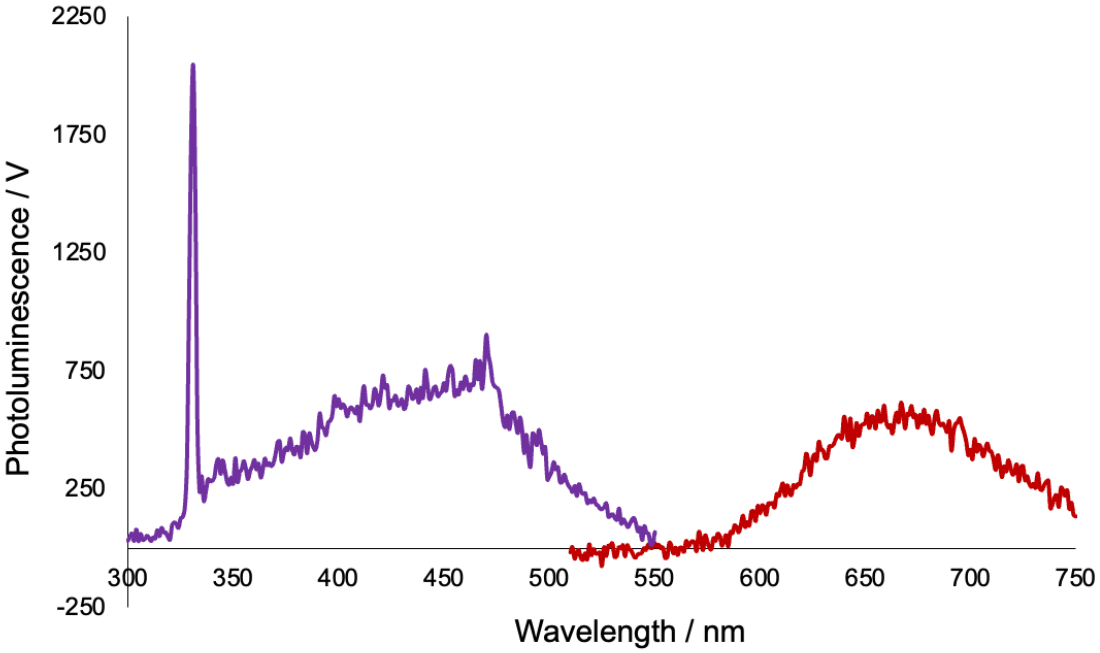

Figure A17. Photoluminescence of *fac*-[$Re(CO)_3$(bpy-5,5'-$(COOH)_2$)Cl] upon excitation at 400 nm (red) and excitation spectrum detected at 660 nm (purple).

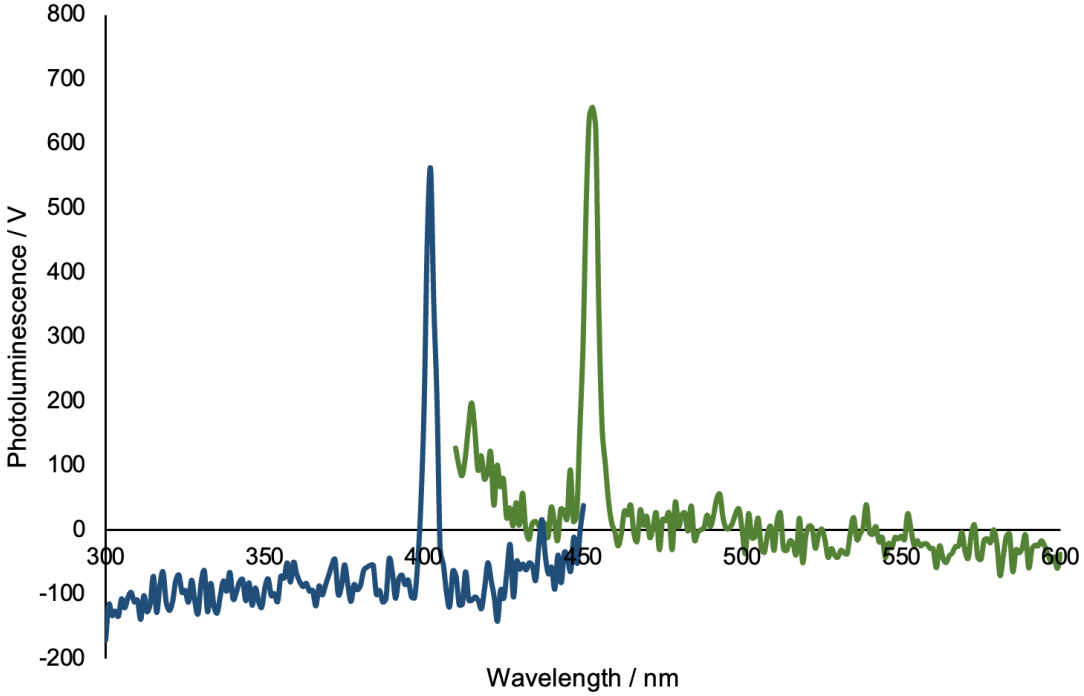

Figure A18. Photoluminescence of fac-[$Re(CO)_3$(5-phen-NO_2)Cl] upon excitation at 400 nm (green) and excitation spectrum detected at 455 nm (blue). No excitation or emission was observed; the sharp bands observed around 400 nm and 455 nm are experimental artifacts.

Crystallographic Data for **9**

The solid-state crystal structure of $[Re(CO)_3(bpy)]_2$ was determined by X-ray diffraction on a Kappa Apex II single-crystal diffractometer.

Table A-1. Crystal data and structure refinement for $[Re(CO)_3(bpy)]_2$.

Empirical Formula	C20 N2 O4 Re
Formula Weight	518.42
Temperature	100(2) K
Wavelength	0.71073 Å
Crystal system, space group	Monoclinic, C 2/c
Unit cell dimensions	a = 13.979(7) Å alpha = 90 deg. b = 10.084(5) Å beta = 105.031(13) deg. c = 17.626(9) Å gamma = 90 deg.
Volume	2400(2) $Å^3$
Z, calculated density	8, 2.870 Mg/m^3
Absorption coefficient	10.167 mm^{-1}
F(000)	1928
Theta range for data collection	2.393 to 24.701 deg.
Limiting indices	-11≤h≤9, -2≤k≤11, -20≤l≤13
Reflections collected / unique	977 / 629
Refinement method	Full-matrix least-squares
Data/restraints/parameters	977 / 0 / 172
Goodness-of-fit on F^2	0.858
Final R indices	R1 = 0.1086, wR2 = 0.2248
R indices (all data)	R1 = 0.0672, wR2 = 0.1754
Largest diff. peak and hole	2.685 and -1.954 e. $Å^{-3}$

Table A-2. Bond lengths (Å) for $[Re(CO)_3(bpy)]_2$.

Re1 C8	1.94(5)
Re1 N2	2.13(4)
Re1 C10	2.03(7)
Re1 C9	2.04(7)
Re1 N1	2.21(6)
Re1 Re1	3.111(4)
N2 C3	1.33(6)
N2 C2	1.39(11)
N1 C6	1.35(5)
N1 C1	1.38(6)
C6 C7	1.38(11)
C3 C4	1.46(7)
C2 C5	1.44(8)

C2 C1	1.46(7)
C5 C13	1.38(8)
C7 C12	1.41(7)
C4 C13	1.46(13)
C1 C11	1.41(12)
C8 O5	1.13(5)
C9 O6	1.09(8)
C10 O7	1.02(6)
C12 C11	1.38(7)

Table A-3. Bond angles (deg.) for $[Re(CO)_3(bpy)]_2$.

C8 Re1 N2	175(3)
C8 Re1 C10	88(2)
N2 Re1 C10	96.0(18)
C8 Re1 C9	87(2)
N2 Re1 C9	95(2)
C10 Re1 C9	89(3)
C8 Re1 N1	100(2)
N2 Re1 N1	77(2)
C10 Re1 N1	100(2)
C9 Re1 N1	169(2)
C8 Re1 Re1	84.6(14)
N2 Re1 Re1	92.0(12)
C10 Re1 Re1	165.8(19)
C9 Re1 Re1	78.7(18)
N1 Re1 Re1	93.7(11)
C3 N2 C2	118(5)
C3 N2 Re1	126(5)
C2 N2 Re1	115(3)
C6 N1 C1	125(5)
C6 N1 Re1	120(4)
C1 N1 Re1	115(3)
N1 C6 C7	117(4)
C4 C3 N2	122(7)
C5 C2 C1	117(6)
C5 C2 N2	124(5)
C1 C2 N2	119(4)
C2 C5 C13	117(7)
C12 C7 C6	121(6)
C3 C4 C13	119(5)
C11 C1 N1	118(4)
C11 C1 C2	128(5)
N1 C1 C2	114(5)
O5 C8 Re1	170(7)
O6 C9 Re1	175(6)
O7 C10 Re1	170(7)
C7 C12 C11	120(7)

C1 C11 C12	119(7)
C5 C13 C4	119(6)

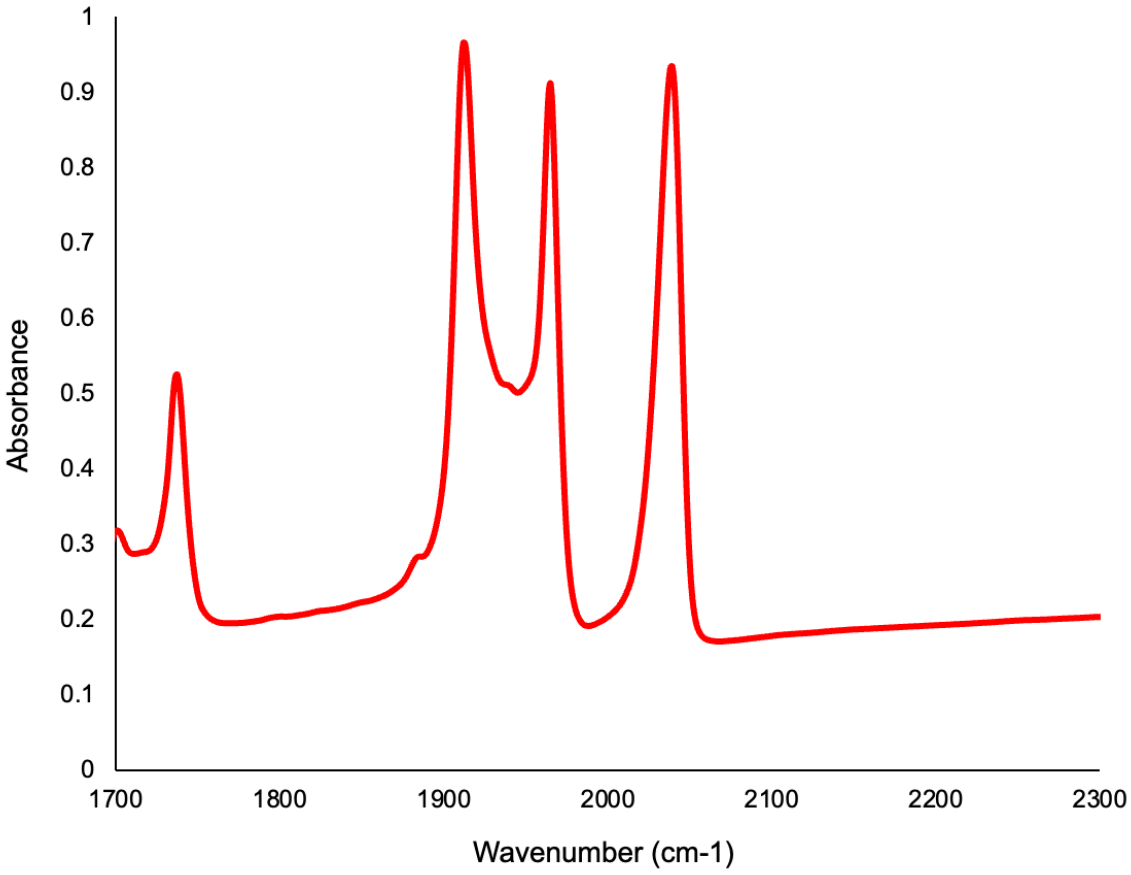

Figure A19. IR spectrum of *fac*-$Mn(CO)_3(4,4'\text{-}(COOH)_2\text{-bpy})Br$ in a mineral oil mull in KBr plates. ν_{CO} = 1914, 1966, 2040 cm^{-1}.